

Secrecy Rate Maximization for Hardware Impaired Untrusted Relaying Network with Deep Learning

Hamed Bastami, Majid Moradikia, Hamid Behroozi, *Member, IEEE*,

Rodrigo C. de Lamare, *Senior Member, IEEE*, Ahmed Abdelhadi, *Senior Member, IEEE*,

and Zhigou Ding, *Fellow, IEEE*

Abstract

This paper investigates the physical layer security design of an untrusted relaying network where the source node coexists with a multi-antenna eavesdropper (Eve). While the communication relies on untrustworthy relay nodes to increase reliability, we aim to protect the confidentiality of information against combined eavesdropping attacks performed by both untrusted relay nodes and Eve. Taking into account the hardware impairments, and power budget constraints, this paper presents a novel approach to jointly optimize relay beamformer and transmit powers aimed at maximizing average secrecy rate (ASR). The resultant optimization problem is non-convex, and a suboptimal solution is obtained through the sequential parametric convex approximation (SPCA) method. In order to prevent any failure due to infeasibility, we propose an iterative initialization algorithm to find the feasible initial point of the original problem. To satisfy low-latency as one of the main key performance indicators (KPI) required in beyond 5G (B5G) communications, a computationally efficient data-driven approach is developed exploiting a deep learning model to improve the ASR while the computational burden is significantly reduced. Simulation results assess the effect of different system parameters on the ASR performance as well as the effectiveness of the proposed deep learning solution in large-scale cases.

Index Terms

Physical layer security, Untrusted relay, Passive eavesdropper, Hardware impairments, Deep learning.

H.Bastami, H.Behroozi, and Majid Moradikia are with the Department of Electrical Engineering, Sharif University of Technology, Tehran, Iran, e-mails: hamed.bastami.ee.sharif.edu, behroozi@sharif.edu, m.moradikia@sutech.ac.ir.

RC de Lamare is with the Telecommunications Research (CETUC) PUC-Rio and University of York, e-mail: delamare@cetuc.puc-rio.br.

Ahmed Abdelhadi is with the Hume Center for National Security and Technology, Virginia Tech, Arlington, VA, 22203 USA, e-mail: aabdelhadi@vt.edu.

Zhigou Ding is with School of Electrical and Electronic Engineering, The University of Manchester, Manchester, M13 9PL, UK, e-mail: zhiguo.ding@manchester.ac.uk.

I. INTRODUCTION

IN the last decades, physical layer security (PLS) has attracted a significant interest as a promising paradigm for establishing secure communication against unfriendly eavesdroppers (Eves). Unlike the conventional sophisticated cryptographic techniques, implemented in the upper layers, PLS provides the secure communication by intelligently exploiting the time varying nature of fading channels [1]. In this regard, Wyner showed as long as the channel condition of Eve is a degraded version of the intended receiver, we can hinder the Eve to overhear the information while the intended receiver can correctly decode the information from the received signal [2]. As a result, relay-assisted communication has recently gained much interest [3]-[15] as an effective PLS solution. In order to take advantages of multiple intermediate helpers, i.e., cooperative beamforming (CB) and cooperative jamming (CJ), have been extensively proposed in the literature [3]-[15]. The main idea of CB is to adjust the weights at distributed relay nodes for focusing a narrow beam on the legitimate receiver [7], [14] or nulling out the relayed information at potential Eve, i.e., null space beamforming (NSB) [3]-[6], [8]-[12]. In contrast, CJ helps to confuse Eves by isotropically radiating interference artificial noise (AN) signal [3]-[6], [8]-[14]. Besides cooperative relay nodes, the usage of destination-aided CJ (DACJ) can lead to the legitimate destination playing the role of a jammer [12]-[14]. Notably, when the CJ and CB techniques are incorporated together, enhanced secrecy is achieved [3]-[6], [8]-[12]. In particular, DACJ can generally achieve a higher secrecy rate than that obtained by deploying one or multiple relay nodes to emit jamming noises [12]. In fact, by applying DACJ, we can take full advantage of the relay nodes to amplify and forward (AF) the source signal rather than sacrificing a relay node and reducing array gain.

In some practical scenarios such as internet of things (IoT) networks, a curious node can collaborate as a helper node. Although this untrustworthy relay node is deployed to improve the communication reliability, it may attempt to wiretap the information which should be taken into account as a potential passive attack [8], [12], [15]. To address the security concern of an untrusted relaying network in the presence of a single-antenna external Eve, a joint CB and CJ design was presented in [8] to the secrecy rate maximization. However, the authors of [8] considered the ideal hardware, which is not realistic in practice. The impact of the inherent imperfection namely hardware impairment (HI), as a more realistic scenario was taken into account in [11], [14]. In particular, in [11], a different joint CB-CJ scheme was proposed. Actually, given the common assumption of unknown Eve's CSI [11], [12], [14], [15], the secrecy rate maximization problem does not work anymore and therefore it is replaced by another tractable optimization problem in

which the power assigned for information transmission is minimized such that it needs to be sufficient for satisfying the minimum required quality of service (QoS) at the destination. Hence the remainder power budget can be allocated to maximize the jamming sources in order to enhance the security of the system. This design leads to a sub-optimal but adequate solution.

In this paper, we assume perfect CSI at the transmitter (CSIT) and the receiver (CSIR).¹ It should be noted that the assumption of perfect CSI knowledge is ideal, however, the result obtained in this paper provides the performance limit for practical HI relaying communication systems. Given these cases, despite the adequate PLS design proposed by [11], the maximized secrecy rate cannot be achieved. Additionally, regarding the solution proposed in [8], although the authors presumed the external Eve, having known CSI, they considered unrealistic assumptions of sum power constraint at the relays together with perfect hardware. Moreover, because of the single antenna Eve, considered in [8], the proposed design cannot be generalized to more difficult scenarios, in the sense of security, where the Eve has been equipped with multi-antenna.

This paper goes beyond the two abovementioned studies of [8] and [11] by investigating a joint CB-CJ design with the goal of secrecy rate maximization. More explicitly, by considering realistic HIs in an untrusted cooperative network in the presence of a multi-antenna external Eve, the relay beamformer and transmit powers are jointly designed so that the achievable secrecy rate (ASR) is maximized. For this problem, both the total power budget constraint for the whole network and individual power constraint at each node, are considered. To combat the combined eavesdropping attacks by untrusted nodes and external Eve, the DACJ is selected for the first phase and the idle source node is firstly configured to serve as the jammer for the second phase. As the formulated optimization problem is non-linear and non-convex, that is NP-hard, the alternative solution is to deploy NSB at the cooperative relay nodes to cancel out the information leakage at Eve, resulting in a simpler non-convex optimization problem. Thanks to NSB the second cooperative phase is secured and we no longer need to employ jamming and thus the source node, which was earlier activated to serve as a jammer in the second phase, might remain silent during this phase. To solve the corresponding optimization problem we resort to the sequential parametric convex approximation (SPCA) methodology [19], [20], leading to a tradeoff between computational complexity and optimality of the solution. SPCA results in an iterative algorithm wherein the non-convex feasible

¹To practice, there are many practical scenarios where the Eve's CSI is available. This assumption corresponds to the scenarios where Eve is one of the network's users, but has not been authorized to receive the current services offered by the source [5], [6], [8]. Furthermore, even for a passive Eve, due to the local oscillator power inadvertently leaked from the receiver RF front-end, Eve's CSI can be estimated [18].

set is suitably approximated by a convex feasible set at each iteration. Using this convex approximation, a sequence of convex programs can be efficiently solved, instead. In order to prevent any failure due to infeasibility we also develop an iterative initialization algorithm to find the feasible initial point of the original problem instead of an arbitrary point, as in the conventional SPCA [19], [20]. Despite the excellent results, the computational complexity order of numerical SPCA-based solution is significantly increased upon increasing the network dimension including the number of users, relay nodes, and number of antennas equipped at each node. This will be verified both analytically and through simulation results in this paper.

Satisfying low-latency requirement, as one of the main Key Performance Indicators (KPIs) of beyond 5G (B5G) [23] communications, would be specifically challenging in face of high computational load due to large-scale scenarios. To circumvent this issue, artificial intelligence (AI)-enabled communications comes into prominence. A subset of key-enabling technologies of AI, so-called deep learning (DL), is key due to its nonlinear modeling ability to solve complicated problems. To be specific, the stronger computing rate and lower price of deep neural networks (DNN) make it more practical in wider scenarios, e.g., system performance analysis [26] and wireless resource management [27]-[31]. Given the capability of DNN in reducing the computational cost, we have developed a DL-based approach to solve the non-convex optimization problem. In the proposed DL approach, the DNN model is firstly trained to extract a relationship between the system parameters and optimization variables. Using this relationship, the ASR performance can be efficiently predicted.

In summary, the main contributions of this paper are:

- Taking into account the HIs, and both the total power budget constraint for the whole network and individual power constraint at each node, we propose a novel approach to jointly optimizing the relay beamformer and transmit powers aimed at maximizing the ASR. While to safeguard the first transmission phase the DACJ strategy is opted, the security of the second phase is guaranteed by deploying NSB at the relay nodes.
- To maximize the ASR, an iterative algorithm is proposed through solving the non-convex optimization problem iteratively. We use the SPCA method to obtain a suboptimal solution. Moreover, to avoid any failure due to infeasibility, an initialization algorithm is proposed to find the feasible initial point of the original problem.
- Despite the similar scenario in [11] with unknown Eve's CSI assumption, our numerical results show

that its performance is significantly lower compared to the performance of the proposed approach. This is because the proposed approach directly maximizes the ASR and considerably outperforms the approach in [11]. Therefore, our proposed scheme can be regarded as an upper bound though some relaxation is adopted to overcome the nonconvexity.

- Due to unknown Eve's CSI assumption in [11], a relay selection algorithm, namely hybrid assisted cooperative jamming (HACJ), which selects the jammer node among relay nodes and destination, is needed to improve the secrecy. However, we can get rid of the computational load imposed by relay selection using simple DACJ, achieving better performance than HACJ. This is because, assuming perfect CSIT and CSIR, instead of choosing a relay node as a jammer the entire potential of relay nodes are preferred to forming a centralized beam towards the legitimate destination whilst completely nulling out the leakage at Eve.
- To deal with high computational load imposed by large-scale scenarios, a deep learning-based approach is also proposed where a DNN model is trained to extract a relationship between the system parameters and optimization variables. Using this relationship, the ASR performance can be efficiently predicted and maximized. This model can be generalized to various optimization problems, leading to SPCA-based solution.

The rest of this paper is organized as follows. The system model is provided in Section II. Section III presents the problem formulation and the corresponding optimization problem. Section IV obtain the proposed SPCA-based solution and converts the non-convex problem into a convex problem. The feasible initialization procedure is provided in Section V. The deep learning scheme with the aim of reducing the computational cost in large-scale scenarios is presented in section VI. Complexity analysis of the proposed scheme is evaluated in Section VII. In Section VIII, simulation results are presented to show the effectiveness of the proposed method, and finally the paper is concluded in Section IX.

Notation: Vectors and matrices are denoted by lower-case and upper-case boldface symbols, respectively. $(\cdot)^T$, $(\cdot)^*$, $(\cdot)^H$, and $(\cdot)^{-1}$ denote the transpose, conjugate, conjugate transpose, and inverse of a matrix respectively. $\Re(\cdot)$ denote the real part of a complex variable, and $\Im(\cdot)$ denote the imaginary part of a complex variable. We use $\mathbb{E}\{\cdot\}$ and \triangleq to denote the expectation and definition operations, respectively. A complex Gaussian random variable with mean μ and variance σ^2 reads as $\mathcal{CN}(\mu, \sigma^2)$. Notation $\text{Vec}(\mathbf{H})$ convert matrix \mathbf{H} in single column vector, and \mathbf{I}_N denotes $N \times N$ identity matrix. Also, $\mathbb{R}^{N \times 1}$ and $\mathbb{C}^{N \times 1}$ denote the set of real and complex N -dimensional vector, respectively. $\mathbb{C}^{N \times N}$ stands for an $N \times N$ complex

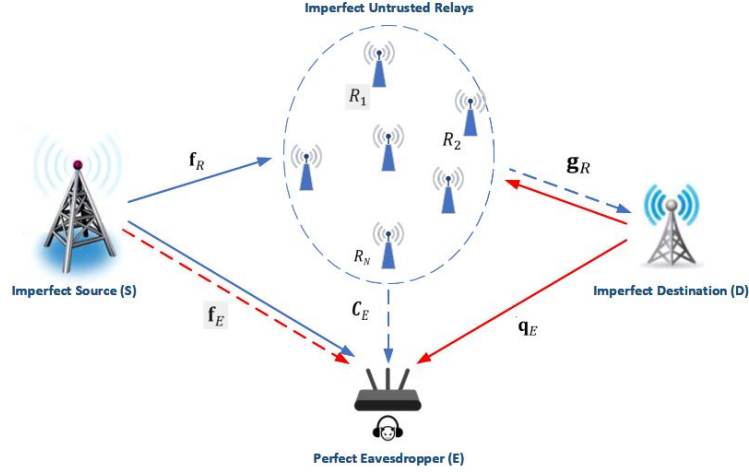


Fig. 1. The considered cooperative network.

matrix.

II. SYSTEM MODEL

A wireless network is considered, as shown in Fig.1, in which a source node (S) aims to convey the confidential message to a legitimate destination (D) with the aid of N distributed intermediate relay node available in the set of $\mathbf{R} \triangleq \{R_i\}_{i=1}^N$, in the presence of an external eavesdropper E . The relay nodes in our network are semi-trusted [8], i.e., they are trusted to send the accurate CSIs to S via relay's cooperation while they are untrustworthy for retransmitting the confidential information. It is noteworthy that the term “*curious node*” throughout the paper comprises both the untrusted relay nodes and external Eve. We further assume that the untrusted relays are deployed in non-colluding settings. Besides, given that all nodes are subjected to the half-duplex constraint and also there is no direct connection between S and D , data transmission takes place in two consecutive time-slots. We suppose that E is equipped with N_E antenna while all the other nodes have a single antenna. In our study, all the channels are modelled as block-fading with channel reciprocity [9]. In phase I, while S broadcasts the information signal with power $0 < P_s \leq P_T$, the destination node (D) is configured to send the interference signal with power $0 < P_{J_1} \leq \bar{P}_{J_1}$ with the aim of confusing the curious nodes. During the second phase of transmission, called relaying phase, the untrusted amplify-and-forward (AF) relays within set \mathbf{R} adopt the distributed beamforming to forward the received signal towards the legitimate terminal D . The power consumed by \mathbf{R} is represented by the vector $\mathbf{P}_R \triangleq [P_{R_1}, P_{R_2}, \dots, P_{R_N}]^T \in \mathbb{R}^{N \times 1}$, and P_{R_l} therein denotes the power consumption at l -th relay node R_l , $\forall l \in \mathcal{L}$ with $\mathcal{L} \triangleq \{1, 2, \dots, N\}$. Notably, in the relaying

phase, although the untrusted relays cannot decipher the information, they provide another chance for E to extract the information. As such, we should secure the system only against the Eve in this phase. Hence, in the relaying phase in order to combat the eavesdropper's attack, we deploy the source node (S) for injecting jamming signal with power $0 < P_{J_2} \leq \bar{P}_{J_2}$.

The statistical behaviour of HI at node $i \in \{S, \mathbf{R}, D\}$ is characterized by exploiting the generalized system model of [10]. Note that the ideal hardware eavesdropper is considered in this paper which implies the worst-case condition in terms of secrecy performance. Accordingly, denoting the impairment levels at Tx and Rx segments respectively by the so-called error vector magnitude (EVM)² parameters k_i^t and k_i^r , defined as the ratio of the average distortion magnitude to the average of signal magnitude, the distortion noise appeared at each node are presented as: **i.** $\eta_s^t \sim \mathcal{CN}(0, P_s k_s^{t2})$, **ii.** $\eta_{J_1}^t \sim \mathcal{CN}(0, P_{J_1} k_{J_1}^{t2})$, **iii.** $\eta_{J_2}^t \sim \mathcal{CN}(0, P_{J_2} k_{J_2}^{t2})$, **iv.** $\eta_D^r \sim \mathcal{CN}(0, k_D^r \sum_{i=1}^N P_{R_i} |g_{R_i}|^2)$, **v.** $\boldsymbol{\eta}_R^r \sim \mathcal{CN}(0, k_R^r \mathbf{\Pi}(P_s, P_{J_1}))$, **vi.** $\boldsymbol{\eta}_R^t \sim \mathcal{CN}(0, k_R^t \mathbf{\Lambda}(\mathbf{P}_R))$, where: $\mathbf{\Lambda}(\mathbf{P}_R) \triangleq \text{diag}(\mathbf{P}_R)$, and

$$\begin{aligned} \mathbf{\Pi}(P_s, P_{J_1}) &\triangleq \text{diag} \left[(P_s |f_{R1}|^2 + P_{J_1} |g_{R1}|^2), \right. \\ &\quad \left. \dots, (P_s |f_{RN}|^2 + P_{J_1} |g_{RN}|^2) \right], \end{aligned}$$

where $\mathbf{f}_R \triangleq [f_{R,1}, f_{R,2}, \dots, f_{R,N}]^T$ and $\mathbf{g}_R \triangleq [g_{R,1}, g_{R,2}, \dots, g_{R,N}]^T$ represent the complex-valued channel coefficients from the $S \rightarrow \mathbf{R}$ and $\mathbf{R} \rightarrow D$, respectively.

A. Signal Representation

As discussed above, during the first phase, while S broadcasts the unit power information symbol x_s , i.e., $\mathbb{E}\{|x_s|^2\} = 1$, the destination (D) radiates the normalized power jamming signal z_I , i.e., $\mathbb{E}\{|z_I|^2\} = 1$, to cover the information transmission. The signals received at untrusted relay nodes \mathbf{R} , i.e., $\mathbf{y}_R \in \mathbb{C}^{N \times 1}$, and E during phase I, i.e., $\mathbf{y}_E^{(1)} \in \mathbb{C}^{N_E \times 1}$ can be represented by :

$$\mathbf{y}_R = \left(\sqrt{P_s} x_s + \eta_s^t \right) \mathbf{f}_R + \left(\sqrt{P_{J_1}} z_1 + \eta_{J_1}^t \right) \mathbf{g}_R + \boldsymbol{\eta}_R^r + \mathbf{n}_R, \quad (1)$$

$$\mathbf{y}_E^{(1)} = \left(\sqrt{P_s} x_s + \eta_s^t \right) \mathbf{f}_E + \left(\sqrt{P_{J_1}} z_1 + \eta_{J_1}^t \right) \mathbf{q}_E + \mathbf{n}_E^{(1)}, \quad (2)$$

where $\mathbf{f}_E \in \mathbb{C}^{N_E \times 1}$ and $\mathbf{q}_E \in \mathbb{C}^{N_E \times 1}$ denote the complex-valued channel coefficients of the $S \rightarrow E$ and $D \rightarrow E$ links, respectively. $\mathbf{n}_R \in \mathbb{C}^{N \times 1}$ and $\mathbf{n}_E^{(1)} \in \mathbb{C}^{N_E \times 1}$ respectively denote the additive noise at the

²The EVM, can be measured directly in practice [24], e.g., 3GPP LTE has EVM requirements in the range of $k_i^t, k_i^r \in [0.08, 0.175]$.

relay nodes and E in phase I. In relaying phase, the received signal at \mathbf{R} is amplified and forwarded towards D . The transmitted signal by \mathbf{R} is $\mathbf{x}_R = \mathbf{W}^H \mathbf{y}_R$, in which the weight matrix \mathbf{W} is in the form of $\mathbf{W} \triangleq \text{diag}\{\mathbf{w}\}$ with the normalized vector $\mathbf{w} \triangleq [w_1, w_2, \dots, w_N]^T \in \mathbb{C}^{N \times 1}$ and $w_l, \forall l \in \mathcal{L}$, therein indicates the beamforming weight adopted by the l -th relay. In the meantime, as mentioned before, S jams through the unit power jamming signal z_2 . Accordingly, the received signals at D , which decodes the information by self-interference cancellation, and E becomes :

$$y_D = \mathbf{g}_R^T (\mathbf{x}_R + \boldsymbol{\eta}_R^t) + \eta_D^r + n_D = \sqrt{P_s} \mathbf{g}_R^T \mathbf{W}^H \mathbf{f}_R x_s + \bar{n}_D, \quad (3)$$

$$\begin{aligned} \mathbf{y}_E^{(2)} &= \mathbf{C}_E (\mathbf{x}_R + \boldsymbol{\eta}_R^t) + \left(\sqrt{P_{J_2}} z_2 + \eta_{J_2}^t \right) \mathbf{f}_E + \mathbf{n}_E^{(2)} \\ &= \sqrt{P_s} \mathbf{C}_E \mathbf{W}^H \mathbf{f}_R x_s + \sqrt{P_{J_1}} \mathbf{C}_E \mathbf{W}^H \mathbf{g}_R z_1 + \sqrt{P_{J_2}} \mathbf{f}_E z_2 + \bar{\mathbf{n}}_E^{(2)}, \end{aligned} \quad (4)$$

where the l -th column of matrix $\mathbf{C}_E \in \mathbb{C}^{N_E \times N}$, i.e., $\mathbf{C}_{E,l} \in \mathbb{C}^{N_E \times 1}$, denotes the complex-valued channel coefficient from $R_l \rightarrow E$, $\forall l \in \mathcal{L}$. $\bar{n}_D \triangleq \mathbf{g}_R^T \mathbf{W}^H \mathbf{f}_R \eta_s^t + \mathbf{g}_R^T \mathbf{W}^H \mathbf{g}_R \eta_{J_1}^t + \mathbf{g}_R^T \mathbf{W}^H \boldsymbol{\eta}_R^r + \mathbf{g}_R^T \mathbf{W}^H \mathbf{n}_R + \mathbf{g}_R^T \boldsymbol{\eta}_R^t + \eta_D^r + n_D$, and $\bar{\mathbf{n}}_E^{(2)} \triangleq \mathbf{C}_E \mathbf{W}^H \mathbf{f}_R \eta_s^t + \mathbf{C}_E \mathbf{W}^H \mathbf{g}_R \eta_{J_1}^t + \eta_{J_2}^t \mathbf{f}_E + \mathbf{C}_E \mathbf{W}^H \boldsymbol{\eta}_R^r + \mathbf{C}_E \mathbf{W}^H \mathbf{n}_R + \mathbf{C}_E \boldsymbol{\eta}_R^t + \mathbf{n}_E^{(2)}$ and n_D and $\mathbf{n}_E^{(2)} \in \mathbb{C}^{N_E \times 1}$ represent the additive noise at D and E , during the relaying phase, respectively. We normalize the power of z_2 , as well, i.e., $\mathbb{E}\{|z_2|^2\} = 1$ [8].

Note that, \mathbf{x}_R have to meet not only the individual power constraint at each relay node [6], [25] but also the total power constraint of the whole network given by:

$$P_{R_l} = \mathbb{E}\{|x_{R,l}|^2\} \leq Q_l, \forall l \in \mathcal{L}, \quad (5)$$

$$P_{tot} = P_{R,tot} + P_s + P_{J_1} + P_{J_2} \leq Q_{tot}, \quad (6)$$

where $P_{R,tot} = \mathbb{E}\{\mathbf{x}_R^H \mathbf{x}_R\} = \sum_{l=1}^N \mathbb{E}\{|x_{R,l}|^2\}$ stands for the power consumed by \mathbf{R} to retransmit the signal. Q_l denotes the transmit power budget of the l -th relay node, and Q_{tot} is the total power constraint of the whole network. Given that $\mathbf{a}^T \cdot \text{diag}(\mathbf{b}^*) = \mathbf{b}^H \cdot \text{diag}(\mathbf{a})$, by defining $\mathbf{G}_R \triangleq \text{diag}(\mathbf{g}_R)$, one can rewrite Eq. (3) as:

$$y_D = \sqrt{P_s} \mathbf{w}^H \mathbf{G}_R \mathbf{f}_R x_s + \bar{n}_D, \quad (7)$$

The equivalent model for the legitimate node D is a SISO system as shown in (7), whilst E exploits

the information received from both phases to extract the information by incorporating the observations of two phases, as it was obtained in (2) and (4), as follows :

$$\mathbf{y}_E = \mathbf{H}_E x_s + \mathbf{n}_E, \quad (8)$$

where we have:

$$\mathbf{H}_E = \begin{bmatrix} \sqrt{P_s} \mathbf{f}_E \\ \sqrt{P_s} \mathbf{C}_E \mathbf{F}_R \mathbf{w}^* \end{bmatrix}, \quad \mathbf{n}_E = \begin{bmatrix} \bar{\mathbf{n}}_E^{(1)} \\ \sqrt{P_{J_1}} \mathbf{C}_E \mathbf{G}_R \mathbf{w}^* z_1 + \sqrt{P_{J_2}} \mathbf{f}_E + \bar{\mathbf{n}}_E^{(2)} \end{bmatrix}, \quad (9)$$

with $\mathbf{F}_R \triangleq \text{diag}(\mathbf{f}_R)$ and $\bar{\mathbf{n}}_E^{(1)} \triangleq \sqrt{P_{J_1}} \mathbf{q}_E z_1 + \mathbf{f}_E \eta_s^t + \mathbf{q}_E \eta_{J_1}^t + \mathbf{n}_E^{(1)}$. In addition, \mathbf{n}_E is zero-mean Gaussian vector with covariance matrix $\mathbf{Q}_E = \mathbb{E} \{ \mathbf{n}_E \mathbf{n}_E^H \} \in \mathbb{C}^{2N_E \times 2N_E}$. All the local noise terms n_D , $\mathbf{n}_E^{(1)}$, $\bar{\mathbf{n}}_E^{(2)}$ and \mathbf{n}_R are zero-mean and independent complex Gaussian random variables (*r.v.s*) with variance σ^2 . Both the jamming signals z_1 and z_2 are assumed to be complex Gaussian *r.v.s*, as well.

The end-to-end information rate $I(y_D; x_s)$ achieved by the legitimate terminal is given by:

$$I(y_D; x_s) = \frac{1}{2} \log_2 \left(1 + \frac{P_s \mathbf{w}^H \Phi_{Gf} \mathbf{w}}{\mathbf{w}^H \Psi_k(P_s, P_{J_1}) \mathbf{w} + \tau_{RD} \mathbf{g}_R^T \Lambda(\mathbf{P}_R) \mathbf{g}_R^* + \sigma^2} \right), \quad (10)$$

with $\Psi_k(P_s, P_{J_1}) \triangleq P_{J_1} k_{J_1}^t{}^2 \Phi_{Gg} + P_{J_1} k_R^r{}^2 \Phi_{GG} + P_s k_s^t{}^2 \Phi_{Gf} + P_s k_R^r{}^2 \Phi_{GF} + \sigma^2 \Phi_G$, with $\Phi_{Gf} \triangleq \mathbf{G}_R \mathbf{f}_R \mathbf{f}_R^H \mathbf{G}_R^H$, $\Phi_{Gg} \triangleq \mathbf{G}_R \mathbf{g}_R \mathbf{g}_R^H \mathbf{G}_R^H$, $\Phi_{GG} \triangleq \text{diag}(|g_{R1}|^4, \dots, |g_{RN}|^4)$, $\Phi_{GF} \triangleq \mathbf{G}_R \mathbf{F}_R \mathbf{F}_R^H \mathbf{G}_R^H$, $\Phi_G \triangleq \mathbf{G}_R \mathbf{G}_R^H$, and $\tau_{RD} \triangleq k_R^t{}^2 + k_D^r{}^2$.

The information leakage at R_l , i.e., $I(y_{R_l}; x_s)$, is also obtained as:

$$I(y_{R_l}; x_s) = \frac{1}{2} \log_2 (1 + \Omega_l^D), \quad (11)$$

where $\Omega_l^D \triangleq \frac{P_s |f_{Rl}|^2}{P_{J_1} \tau_{RJ_1} |g_{Rl}|^2 + P_s \tau_{RS} |f_{Rl}|^2 + \sigma^2}$ with $\tau_{RS} \triangleq k_s^t{}^2 + k_R^r{}^2$ and $\tau_{RJ_1} \triangleq 1 + k_{J_1}^t{}^2 + k_R^r{}^2$, stands for the measured SINR at R_l in the presence of jammer node D .

Notably, while each of the untrusted relays adopts the selection combining (SC) technique to extract the information symbol based on its own observation [8], Eve attempts to get more information through combining its observations from both phases. Hence, considering that Eve sees an equivalent $1 \times 2N_E$ SIMO system, the corresponding information leakage $I(y_E; x_s)$, is:

$$I(y_E; x_s) = \frac{1}{2} \log_2 [\det (\mathbf{I}_{2N_E} + \mathbf{H}_E \mathbf{H}_E^H \mathbf{Q}_E^{-1})], \quad (12)$$

III. PROPOSED SECRECY SCHEME

The security issue can be addressed through maximizing the ASR, yielding the optimal solution. Therefore, the ASR in the presence of both E and untrusted relays is evaluated by [12]:

$$R_s = \max \left[I(y_D; x_s) - \max_{i \in \{\mathbf{R}, E\}} I(y_i; x_s) \right]^+, \quad (13)$$

where $[a]^+ = \max(0, a)$, and $I(\cdot; \cdot)$ denotes the mutual information.

From the perspective of secrecy capacity, the optimal strategy is to maximize R_s , i.e., $R_s^{max} \triangleq \max R_s$, by searching the optimal \mathbf{w} , $\mathbf{P} \triangleq [P_{J_1}, P_{J_2}, P_s]^T$. Along this line, substituting (11)-(13) into (10) yields the objective function which is neither convex nor concave and thus solving the resultant maximization problem will be difficult. Some numerical methods, e.g., the gradient method or the Newton's method, can be utilized to exhaustively search for the local optimum though we cannot guarantee the optimality of the so-obtained solution. To facilitate the joint design over \mathbf{w} , \mathbf{P} , a sub-optimal criteria will be presented in the following section. With the aim of maximizing the secrecy rate, we wish to increase $I(y_D; x_s)$ as much as possible while keeping the information leakage at the curious nodes as small as possible. Towards this end, beamforming by distributed relay nodes should be designed such that the information leakage at E in phase II, will be thoroughly eliminated. These will be fulfilled by designing \mathbf{w} such that it falls into the null space of the equivalent channel of the relay link from S to E , i.e. $\mathbf{C}_E \mathbf{F}_R \mathbf{w}^* = \mathbf{0}$. Thanks to NSB described above, the information leakage at E was completely eliminated in phase II and thus we can set $P_{J_2} = 0$. Therefore, we can shorten the vector of \mathbf{P} to $\bar{\mathbf{P}} \triangleq [P_{J_1}, P_s]^T$. Now, by substituting $\Lambda(\mathbf{P}_R) \triangleq \mathbf{W}^H \Upsilon_k(\bar{\mathbf{P}}) \mathbf{W}$, where we have $\Upsilon_k(\bar{\mathbf{P}}) \triangleq P_s(1 + \tau_{RS}) \mathbf{F}_R \mathbf{F}_R^H + P_{J_1} \tau_{RJ_1} \mathbf{G}_R \mathbf{G}_R^H + \sigma^2 \mathbf{I}_N$, into (11) and after some manipulations (11) and (13) can be reformulated as:

$$I(y_D; x_s) = \frac{1}{2} \log_2 \left(1 + \frac{P_s \mathbf{w}^H \Phi_{Gf} \mathbf{w}}{\mathbf{w}^H \tilde{\Psi}_k(\bar{\mathbf{P}}) \mathbf{w} + \sigma^2} \right), \quad (14)$$

$$I(y_E; x_s) = \frac{1}{2} \log_2 \left(1 + P_s \mathbf{f}_E^H \left(\tau_{J_1} P_{J_1} \mathbf{q}_E \mathbf{q}_E^H + P_s k_s^t \mathbf{f}_E \mathbf{f}_E^H + \sigma^2 \mathbf{I}_{N_E} \right)^{-1} \mathbf{f}_E \right), \quad (15)$$

where, $\tilde{\Psi}_k(\bar{\mathbf{P}}) \triangleq P_{J_1} k_{J_1}^t \mathbf{\Phi}_{Gg} + P_{J_1} k_1 \mathbf{\Phi}_{GG} + P_s k_2 \mathbf{\Phi}_{GF} + P_s k_s^t \mathbf{\Phi}_{Gf} + \sigma^2 k_3 \mathbf{\Phi}_G$ with $k_1 \triangleq \tau_{RD} \tau_{RJ_1} + k_R^r$, $k_2 \triangleq \tau_{RD} (1 + \tau_{RS}) + k_R^r$ and $k_3 \triangleq 1 + \tau_{RD}$. Note that, since the intended receiver knows the channel associated with itself to relays and the weighted coefficients matrix by some channel estimation method, we expect the backward self-interference term is totally canceled at D . However due to existence of HI,

we still witness some terms related to AN z_1 as, i.e., $P_{J_1} k_{J_1}^t {}^2 \Phi_{Gg} + P_{J_1} k_1 \Phi_{GG}$, which hampers the secrecy and cannot be simply eliminated. In the following section, we will describe our proposed joint optimal power allocation and cooperative beamforming (OPA-CB) strategy.

IV. PROPOSED JOINT OPA-CB DESIGN

For simplicity, we first assume that $i^\circ \in \{\mathbf{R}, E\}$ stands for the most curious node at which the highest information leakage has been occurred. Since the information leakage at E in phase II has been omitted, the equations for the case of $i^\circ = E$ will be analogous to the case of $i^\circ = R_l$. Therefore, in the following, we suppose $i^\circ = E$, and the related analyses for the other case $i^\circ = R_l$ will be discussed wherever is needed. Before getting to the proposed joint OPA-CB design, we define $\mathbf{H} \triangleq \mathbf{C}_E \mathbf{F}_R$, and \mathbf{H}_\perp , which is the projection matrix onto the null space of \mathbf{H} , i.e., $\mathbf{w} = \mathbf{H}_\perp \mathbf{v}$ where $\mathbf{v} \in \mathbb{C}^{(N-N_E-1) \times 1}$ is an arbitrary vector. Now, by inserting $\mathbf{w} = \mathbf{H}_\perp \mathbf{v}$ into (14) and subsequently substituting them into (10), subjected to individual and total power constraints, the following optimization problem is formulated:

$$\mathbf{P}_0 : \max_{\mathbf{v}, \bar{\mathbf{P}}} \frac{1}{2} \log_2 \left(\frac{1 + \frac{P_s \mathbf{v}^H \mathcal{U}_{Gf} \mathbf{v}}{\mathbf{v}^H \mathbf{\Gamma}(\bar{\mathbf{P}}) \mathbf{v} + \sigma^2}}{1 + P_s \mathbf{f}_E^H (\tau_{J_1} P_{J_1} \mathbf{q}_E \mathbf{q}_E^H + P_s k_s^t {}^2 \mathbf{f}_E \mathbf{f}_E^H + \sigma^2 \mathbf{I}_{N_E})^{-1} \mathbf{f}_E} \right) \quad (16)$$

s.t.

$$\mathbf{1}_2^T \bar{\mathbf{P}} + \mathbf{v}^H \bar{\mathbf{\Upsilon}}_k(\bar{\mathbf{P}}) \mathbf{v} \leq Q_{tot}, \quad (16-a)$$

$$\mathbf{v}^H \bar{\mathbf{\Upsilon}}_k^{l,l}(\bar{\mathbf{P}}) \mathbf{v} \leq Q_l, \quad \forall l \in \mathcal{L}, \quad (16-b)$$

$$0 < P_{J_1} \leq \bar{P}_{J_1}, \quad 0 < P_s \leq P_T. \quad (16-e)$$

where $\mathcal{U}_{Gf} \triangleq \mathbf{H}_\perp^H \Phi_{Gf} \mathbf{H}_\perp$, $\mathbf{\Gamma}(\bar{\mathbf{P}}) \triangleq \mathbf{H}_\perp^H \tilde{\Psi}_k(\bar{\mathbf{P}}) \mathbf{H}_\perp$, $\bar{\mathbf{\Upsilon}}_k(\bar{\mathbf{P}}) \triangleq \mathbf{H}_\perp^H \mathbf{\Upsilon}_k(\bar{\mathbf{P}}) \mathbf{H}_\perp$, $\bar{\mathbf{\Upsilon}}_k^{l,l}(\bar{\mathbf{P}}) \triangleq \mathbf{H}_\perp^H \mathbf{\Upsilon}_k^{l,l}(\bar{\mathbf{P}}) \mathbf{H}_\perp$, with $\mathbf{\Upsilon}_k^{l,l}(\mathbf{P}) \triangleq P_s (1 + \tau_{RS}) \mathbf{F}_R \mathbf{E}_l \mathbf{F}_R^H + P_{J_1} \tau_{RJ_1} \mathbf{G}_R \mathbf{E}_l \mathbf{G}_R^H + \sigma^2$ and $\mathbf{E}_l \triangleq \text{diag}(\mathbf{e}_l)$ in which the vector \mathbf{e}_l denotes a unit vector whose n -th entry equals to one. The objective function (16) and also the constraints (16-a) and (16-b) are non-convex. As a consequence, the joint optimization problem (16) is NP-hard and finding a global optimum is computationally expensive or even intractable. In this case, computing a local optima via a low-complexity algorithm is more meaningful, in practice. Along this line, resorting to the SPCA [19], the non-convex problem (16) is approximated by a sequence of convex problems that are much easier to be solved.

A. The Proposed SPCA-based Solution

Variables \mathbf{v} , P_{J_1} , and P_s have been coupled with each other which is an impediment in solving the optimization problem (16). To cope with this issue, the following variable transformation is introduced:

$$q_{J_1} \triangleq \frac{1}{P_{J_1}}, \quad q_s \triangleq \frac{1}{P_s}, \quad \text{and} \quad \mathbf{q} \triangleq [q_{J_1}, q_s]^T, \quad (17)$$

With the notation introduced in (17), we can rewrite the power constraints in (16-a) and (16-b) as:

$$\sigma^2 \mathbf{v}^H \mathbf{v} \frac{\tau_{RJ_1} \mathbf{v}^H \mathbf{H}_\perp^H \mathbf{G}_R \mathbf{H}_R^H \mathbf{H}_\perp \mathbf{v}}{q_{J_1}} + \mathbf{1}_2^T \mathbf{q} + \frac{(1 + \tau_{RS}) \mathbf{v}^H \mathbf{H}_\perp^H \mathbf{F}_R \mathbf{F}_R^H \mathbf{H}_\perp \mathbf{v}}{q_s} + \leq Q_{tot}, \quad (18)$$

$$\sigma^2 \mathbf{v}^H \mathbf{v} \frac{(1 + \tau_{RS}) \mathbf{v}^H \mathbf{H}_\perp^H \mathbf{F}_R \mathbf{E}_l \mathbf{F}_R^H \mathbf{H}_\perp \mathbf{v}}{q_s} + \frac{\tau_{RJ_1} \mathbf{v}^H \mathbf{H}_\perp^H \mathbf{G}_R \mathbf{E}_l \mathbf{G}_R^H \mathbf{H}_\perp \mathbf{v}}{q_{J_1}} + \leq Q_l, \forall l \in \mathcal{L}, \quad (19)$$

where the term $\mathbf{1}_2^T \mathbf{q}$, that is the summation of two convex functions, is strictly convex over \mathbf{q} , [21, Sec. 3.2]. On the other hand, we know that the quadratic form $\mathbf{z}^H \mathbf{A} \mathbf{z}$ is convex with respect to the variable \mathbf{z} if the matrix \mathbf{A} is positive semidefinite [21, Sec. 4.2]. Furthermore, for $g > 0$ the quadratic-over-linear function $\frac{\mathbf{z}^H \mathbf{A} \mathbf{z}}{g}$ is jointly convex over the variables (\mathbf{z}, g) [21, sec 3.2.6]. Consequently, given that $\mathbf{H}_\perp^H \mathbf{F}_R \mathbf{F}_R^H \mathbf{H}_\perp \succcurlyeq \mathbf{0}$, $\mathbf{H}_\perp^H \mathbf{G}_R \mathbf{G}_R^H \mathbf{H}_\perp \succcurlyeq \mathbf{0}$, $\mathbf{v}^H \mathbf{H}_\perp^H \mathbf{F}_R \mathbf{E}_l \mathbf{F}_R^H \mathbf{H}_\perp \succcurlyeq \mathbf{0}$, and $\mathbf{v}^H \mathbf{H}_\perp^H \mathbf{G}_R \mathbf{E}_l \mathbf{G}_R^H \mathbf{H}_\perp \succcurlyeq \mathbf{0}$, the power constraints (18) and (19) are jointly convex in (\mathbf{q}, \mathbf{v}) . We remark that, although the constraints (18) and (19) are convex, the objective function is still non-convex. To tackle the nonconvexity, we exploit SPCA. SPCA is an iterative algorithm in which at each iteration the relevant non-convex part is surrogated by a well-suited inner convex subset that approximates the non-convex feasible solution set. The accuracy of this approximation is boosted iteration by iteration. To apply SPCA, the non-convex problem (16) should be first transformed into a suitable form. Thus, by some variable transformations, the problem (16) is converted into the following equivalent problem:

$$\begin{aligned} \mathbf{P}_1 : \quad & \max && \mathcal{D}(t_B, t_E) = \frac{1}{2} \log_2(1 + t_B) - \frac{1}{2} t_E \\ & t_B, t_E, \omega_B, \omega_E, \\ & \beta, \mathbf{q}, \mathbf{v}, a_s, a_{J_1} \end{aligned} \quad (20)$$

s.t.

$$t_E = \log_2 \omega_E, \quad (20 - a)$$

$$t_B = \frac{\omega_B}{a_s + a_{J_1} + \beta \sigma^2 + \sigma^2}, \quad (20 - b)$$

$$\omega_B = \frac{\mathbf{v}^H \mathbf{U}_{Gf} \mathbf{v}}{q_s}, \quad (20 - c)$$

$$a_s = \frac{\mathbf{v}^H \mathbf{Z}_{gf}^k \mathbf{v}}{q_s}, a_{J_1} = \frac{k_1 \mathbf{v}^H \mathcal{U}_{GG} \mathbf{v}}{q_{J_1}}, \quad (20-d)$$

$$\beta = k_3 \mathbf{v}^H \mathcal{U}_G \mathbf{v}, \quad (20-e)$$

$$\omega_E - 1 = \frac{\mathbf{f}_E^H \left(\tau_{J_1} \frac{\mathbf{q}_E \mathbf{q}_E^H}{q_{J_1}} + k_s^{t^2} \frac{\mathbf{f}_E \mathbf{f}_E^H}{q_s} + \sigma^2 \mathbf{I}_{N_E} \right)^{-1} \mathbf{f}_E}{q_s} \quad (20-f)$$

$$\frac{1}{q_s} \leq P_T, \frac{1}{q_{J_1}} \leq \bar{P}_{J_1}, \quad (20-g)$$

$$(18), (19), \quad (20-i)$$

where $\mathbf{Z}_{gf}^k \triangleq k_s^{t^2} \mathbf{H}_\perp^H \Phi_{Gf} \mathbf{H}_\perp + k_2 \mathbf{H}_\perp^H \Phi_{GF} \mathbf{H}_\perp$, $\mathcal{U}_{GG} \triangleq \mathbf{H}_\perp^H \Phi_{GG} \mathbf{H}_\perp$, $\mathcal{U}_G \triangleq \mathbf{H}_\perp^H \Phi_G \mathbf{H}_\perp$.

Since the objective function of \mathbf{P}_1 is a combination of concave function $\log_2(1 + t_B)$ and a linear function t_E , we deal with a concave objective function. However, the equality constraints (20-a)-(20-f) are still non-convex because of having the functions on both sides of the equalities which are not affine. As such, these non-convex equality constraints should be first transformed into the equivalent convex inequality constraints to make it more tractable. Subsequently, the problem (20) becomes:

$$\begin{aligned} \mathbf{P}_2 : \quad & \max \quad \mathcal{D}(t_B, t_E) \\ & t_B, t_E, \omega_B, \omega_E, \\ & \beta, \mathbf{q}, \mathbf{v}, a_s, a_{J_1} \end{aligned} \quad (21)$$

s.t.

$$t_E \geq \log_2 \omega_E, \quad (21-a)$$

$$t_B \leq \frac{\omega_B}{a_s + a_{J_1} + \beta \sigma^2 + \sigma^2}, \quad (21-b)$$

$$\omega_B \leq \frac{\mathbf{v}^H \mathcal{U}_{Gf} \mathbf{v}}{q_s}, \quad (21-c)$$

$$a_s \geq \frac{\mathbf{v}^H \mathbf{Z}_{gf}^k \mathbf{v}}{q_s}, a_{J_1} \geq \frac{\mathbf{v}^H \mathcal{U}_{GG} \mathbf{v}}{q_{J_1}}, \quad (21-d)$$

$$\beta \geq k_3 \mathbf{v}^H \mathcal{U}_G \mathbf{v}, \quad (21-e)$$

$$\omega_E - 1 \geq \frac{\mathbf{f}_E^H \left(\tau_{J_1} \frac{\mathbf{q}_E \mathbf{q}_E^H}{q_{J_1}} + k_s^{t^2} \frac{\mathbf{f}_E \mathbf{f}_E^H}{q_s} + \sigma^2 \mathbf{I}_{N_E} \right)^{-1} \mathbf{f}_E}{q_s}, \quad (21-f)$$

$$\frac{1}{q_s} \leq P_T, \frac{1}{q_{J_1}} \leq \bar{P}_{J_1}, \quad (21-g)$$

$$(18), (19), \quad (21-i)$$

The proof of equivalence between (20) and (21) is provided in Supplementary material, Section IV.³

So far, we have already transformed the non-convex objective function of the original problem into a concave one \mathbf{P}_2 , while the difficulties now lie in the non-convex constraints (21-b)-(21-f). Now, to circumvent the difficulties associated with non-convex constraints (21-c), we first define slack variables

³Due to pages limits, the detailed convergence analysis of SPCA scheme are given in the supplementary document.

$u_1 \triangleq \Re \{ \mathbf{H}_\perp^H \mathbf{G}_R \mathbf{f}_R \}$, $u_2 \triangleq \Im \{ \mathbf{H}_\perp^H \mathbf{G}_R \mathbf{f}_R \}$, and $\mathbf{u} \triangleq [u_1, u_2]^T$, by which it can be reformulated as $\frac{\mathbf{u}^T \mathbf{u}}{q_s} \geq \omega_B$. This form is still non-convex. Concerning the constraint (21-f), because of the convex function $\frac{1}{q_s}$, it cannot be reformulated into an equivalent linear matrix inequality (LMI) [21]. By exploiting Schur complement, it can be shown that (21-f) can be expressed through the following matrix form:

$$\begin{bmatrix} \varpi & m_s \mathbf{f}_E \\ m_s \mathbf{f}_E^H & \omega_E - 1 \end{bmatrix} \succcurlyeq 0, \quad (22)$$

$$m_{J_1} \leq \frac{1}{q_{J_1}}, \quad (23)$$

$$m_s \geq \frac{1}{\sqrt{q_s}}, \quad (24)$$

where $\varpi \triangleq \tau_{J_1} m_{J_1} \mathbf{q}_E \mathbf{q}_E^H + k_s^{t^2} m_s^2 \mathbf{f}_E \mathbf{f}_E^H + \sigma^2 \mathbf{I}_{N_E}$. Based on above change of variables and equivalent constraints (22) and (24), the problem (21) is written into an equivalent form as follows:

$$\mathbf{P}_3 : \max_{\mathbf{x}} \mathcal{D}(t_B, t_E) \quad (25)$$

s.t.

$$t_E \geq \log_2 \omega_E, \quad (25-a)$$

$$\omega_B \geq a_s t_B + a_{J_1} t_B + t_B \beta \sigma^2 + t_B \sigma^2 \quad (25-b)$$

$$u_1 \triangleq \Re \{ \mathbf{H}_\perp^H \mathbf{G}_R \mathbf{f}_R \}, u_2 \triangleq \Im \{ \mathbf{H}_\perp^H \mathbf{G}_R \mathbf{f}_R \}, \mathbf{u} \triangleq [u_1, u_2]^T, \quad (25-c)$$

$$\frac{\mathbf{u}^T \mathbf{u}}{q_s} \geq \omega_B, \quad (25-d)$$

$$a_s \geq \frac{\mathbf{v}^H \mathbf{Z}_{g_f}^k \mathbf{v}}{q_s}, a_{J_1} \geq \frac{\mathbf{v}^H \mathbf{U}_{GG} \mathbf{v}}{q_{J_1}}, \quad (25-e)$$

$$\beta \geq k_3 \mathbf{v}^H \mathbf{U}_G \mathbf{v}, \quad (25-f)$$

$$\frac{1}{q_s} \leq P_T, \frac{1}{q_{J_1}} \leq \bar{P}_{J_1}, \quad (25-g)$$

$$(18), (19), (22), (23), (24) \quad (25-h)$$

where $\mathbf{x} \triangleq [t_B, t_E, \omega_B, \omega_E, \mathbf{u}, \beta, \mathbf{q}, \mathbf{v}, a_s, a_{J_1}, m_s, m_{J_1}]^T$. Because of the nonconvexity of the constraints (25-a)-(25-f) and (23), the problem (25) is still non-convex. As such, to prepare (25) for using SPCA, we first construct a suitable inner convex subset to approximate the non-convex feasible solution set. Along this line, if we denote the optimal solutions of the convex approximation program at the $(i-1)$ -th iteration by $\omega_E(i-1)$, $a_s(i-1)$, $a_{J_1}(i-1)$, $t_B(i-1)$, $\beta(i-1)$, $\mathbf{u}(i-1)$, $q_{J_1}(i-1)$, and $q_s(i-1)$, these non-convex constraints (25-a)-(25-f) and (23) can be approximated by their first-order Taylor approximations

Algorithm 1 Joint OPA-CB design algorithm:

Input: Set the threshold value for accuracy (δ_I) and the maximum number of iterations (N_{max})

Initialization: Initialize $\mathbf{x}^{(0)}$. Set the iteration number $i = 0$

Calculating the optimal: $P_s^\circ, P_{J_1}^\circ, \mathbf{v}^\circ$

While $\left\{ \left| \mathcal{D} \left(t_B^{(i+1)}, t_E^{(i+1)} \right) - \mathcal{D} \left(t_B^{(i)}, t_E^{(i)} \right) \right| \leq \delta_I \text{ or} \right.$
 $\left. i \leq N_{max} \right\}$

do (1) to (4):

(1). Calculate (26)-(29),

(2). Solve (30), then assign the solution to $\mathbf{x}^{(i+1)}$,

(3). Update the slack variables $\gamma(i), \theta(i), \rho(i)$ based on $\mathbf{x}^{(i+1)}$,

(4). $i = i + 1$

End While,

Output: $P_s^\circ, P_{J_1}^\circ, \mathbf{v}^\circ$

around the optimal solutions at the $(i - 1)$ -th iteration, and their equivalent are respectively given in (26)-(29), as follow:

$$\Gamma(\omega_E, \omega_E(i-1)) \triangleq \log_2(\omega_E(i-1)) + \frac{\omega_E - \omega_E(i-1)}{\omega_E(i-1) \cdot \ln(2)} \leq t_E, \quad (26)$$

$$F(t_B, a_s, a_{J_1}, \beta, \gamma(i), \theta(i), \rho(i), \omega_B) \triangleq \Xi(t_B, a_s, \theta(i)) + \Xi(t_B, a_{J_1}, \rho(i)) + \Xi(t_B, \beta, \gamma(i)) \sigma^2 + t_B \sigma^2 - \omega_B \leq 0, \quad (27)$$

$$\mathcal{S}(\mathbf{u}, q_s; \mathbf{u}(i-1), q_s(i-1)) \triangleq \frac{\mathbf{u}(i-1)^T \mathbf{u}(i-1)}{q_s(i-1)} \times \left(1 - \frac{q_s - q_s(i-1)}{q_s(i-1)} \right) + \frac{2\mathbf{u}(i-1)^T}{q_s(i-1)} (\mathbf{u} - \mathbf{u}(i-1)) \geq \omega_B, \quad (28)$$

$$\mathcal{T}(q_{J_1}, q_{J_1}(i-1)) \triangleq \frac{1}{q_{J_1}(i-1)} \left(1 - \frac{q_{J_1} - q_{J_1}(i-1)}{q_{J_1}(i-1)} \right) \geq m_{J_1}, \quad (29)$$

where, $\Xi(x_1, x_2, \lambda) \triangleq \frac{\lambda}{2} x_1^2 + \frac{1}{2\lambda} x_2^2$, $\theta(i) \triangleq \frac{a_s(i-1)}{t_B(i-1)}$, $\rho(i) \triangleq \frac{a_{J_1}(i-1)}{t_B(i-1)}$, $\gamma(i) \triangleq \frac{\beta(i-1)}{t_B(i-1)}$. Given the above approximations, the proposed iterative algorithm for the joint OPA-CB design is presented in Algorithm I, in which the following convex optimization is solved at the i -th iteration:

$$\mathbf{P}_i : \max_{\mathbf{x}} \mathcal{D}(t_B, t_E) \quad (30)$$

Algorithm 2 The proposed SPCA-based FIPSA:

Input: Set the threshold value for accuracy (δ_ϵ) and the maximum number of iterations (M_{max})

Initialization: Initialize with an arbitrary random point $\mathbf{x}^{(0)}$ and set the iteration number $i = 0$

While $\{ |s^{(i+1)} - s^{(i)}| \leq \delta_\epsilon \text{ or } i \leq M_{max} \}$ **do (1) to (3):**

(1). Calculate (26)-(29),

(2). Solve the problem (31),

(3). $i = i + 1$

End While,

Output: $\mathbf{x}^\circ, s^\circ$.

s.t.

$$(26)-(29), (18), (19), (22), (24) \quad (30 - a)$$

$$a_s \geq \frac{\mathbf{v}^H \mathbf{z}_{qf}^k \mathbf{v}}{q_s}, a_{J_1} \geq \frac{\mathbf{v}^H \mathcal{U}_{GG} \mathbf{v}}{q_{J_1}}, \quad (30 - b)$$

$$\beta \geq k_3 \mathbf{v}^H \mathcal{U}_G \mathbf{v}, \quad (30 - c)$$

$$\frac{1}{q_s} \leq P_T, \frac{1}{q_{J_1}} \leq \bar{P}_{J_1},^4 \quad (30 - d)$$

Note that, the iterative process will proceed until some stopping criteria is satisfied or the maximum predefined number of iterations N_{max} is reached. The convergence of the algorithm is investigated in Supplementary material.

B. SPCA-based Feasible Initial Points Search Algorithm (FIPSA)

If the feasible initial points exist for the problem (30), the points acquired by (30) at each iteration, definitely fall into the feasible set introduced by the original problem (25) (see Supplementary material, Lemma 2). However, the feasible initial point may not be found easily, in general and thus the algorithm may fail at the first iteration owing to infeasibility. Hence, developing an algorithm to find a feasible initial point is required. To do so, another optimization problem is solved in which the real-valued slack parameter $s \geq 0$ is minimized. This parameter can be interpreted as the infeasibility indicator thereby the violation of constraints of problem (30-a)-(30-b) is measured. The feasibility problem is given by:

$$\mathbf{P}_5 : \min_{\mathbf{x}} s \quad (31)$$

s.t.

$$\Gamma(\omega_E, \omega_E(i-1)) \leq -s, \quad (31-a)$$

$$F(t_B, a_s, a_{J_1}, \beta, \gamma(i), \theta(i), \rho(i), \omega_B) \leq -s, \quad (31-b)$$

$$\mathcal{S}(\mathbf{u}, q_s; \mathbf{u}(i-1), q_s(i-1)) \leq -s, \quad (31-c)$$

$$\mathcal{T}(q_{J_1}, q_{J_1}(i-1)) \leq -s, \quad (31-d)$$

$$\frac{1}{\sqrt{q_s}} - m_s \leq -s, \quad (31-e)$$

$$\begin{bmatrix} \boldsymbol{\omega} & m_s \mathbf{f}_E \\ m_s \mathbf{f}_E^H & \omega_E - 1 \end{bmatrix} \succcurlyeq s, \quad (31-f)$$

$$\frac{\mathbf{v}^H \mathbf{Z}_{gf}^k \mathbf{v}}{q_s} - a_s \leq -s, \quad \frac{\mathbf{v}^H \mathcal{U}_{GG} \mathbf{v}}{q_{J_1}} - a_{J_1} \leq -s, \quad (31-g)$$

$$k_3 \mathbf{v}^H \mathcal{U}_G \mathbf{v} - \beta \leq -s, \quad (31-h)$$

$$\frac{1}{q_s} - P_T \leq -s, \quad \frac{1}{q_{J_1}} - \bar{P}_{J_1} \leq -s, \quad (31-i)$$

$$s \geq 0, \quad (31-j)$$

The optimal solution of the problem (31) at the $(l-1)$ -th iteration is a feasible solution of the problem (31) at the l -th iteration. Therefore, the optimal value of the objective function in the problem (31) is non-increasing as the iteration number l increases (see Lemma 2 – (ii)). Algorithm 2 is guaranteed to converge.

The SPCA-based feasible initial point search algorithm is presented in Algorithm 2. Unlike Algorithm 1, where we assumed that it is initialized with a feasible point, Algorithm 2 begins with an arbitrary random point. The algorithm will proceed unless the difference of objective value s in two consecutive iterations becomes smaller than the predefined threshold value, i.e., $\left| \mathcal{D}(t_B^{(i+1)}, t_E^{(i+1)}, t_B, t_E) - \mathcal{D}(t_B^{(i)}, t_E^{(i)}, t_B, t_E) \right| \leq \delta_\epsilon$ or the maximum number of affordable iterations is reached. Besides, whenever the objective value becomes zero the algorithm ceases. Hence, after calculating the feasible initial points through Algorithm 2, the optimal values of P_s° , $P_{J_1}^\circ$, \mathbf{v}° are obtained via Algorithm 1. If no feasible point is obtained for some system parameters, they should be relaxed so that a feasible solution is achieved.

V. PROPOSED DEEP LEARNING SCHEME

Facing with high computational load in large-scale scenarios, the computational complexity order of numerical SPCA-based solution (30) is significantly increased upon increasing the network dimension including N and N_E . Unlike the complex iterative process of the SPCA-based scheme, in the DNN-based scheme, a multi-layer model is replaced, where each layer includes some simple matrix multiplication and summation operations followed by a non-linear mapping, i.e., activation function. This structure

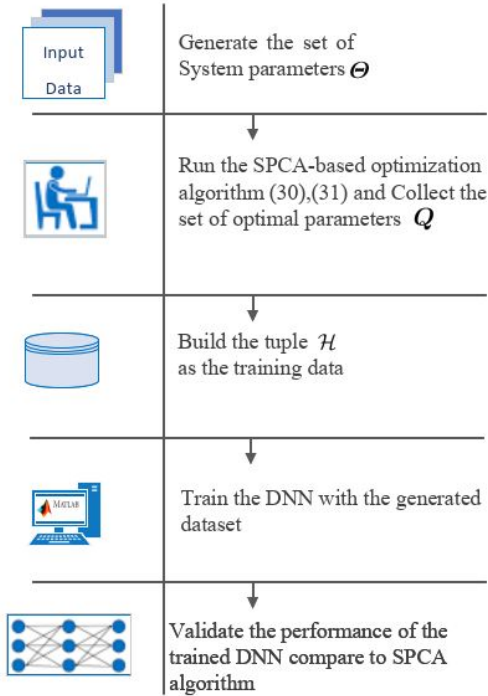


Fig. 2. The process of the proposed DNN-based scheme.

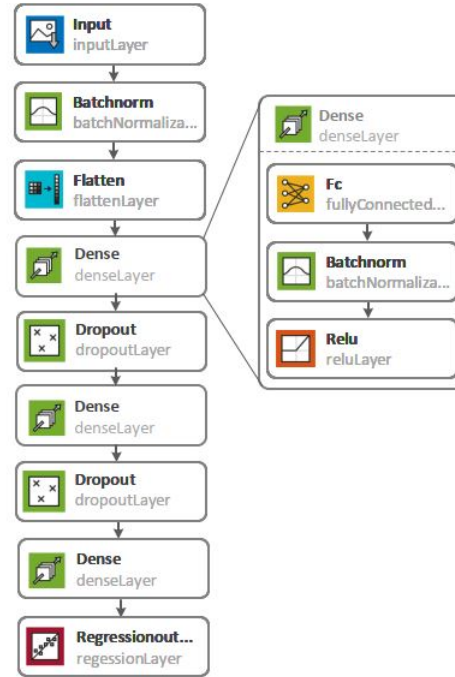


Fig. 3. Proposed DNN framework

guarantees the real-time performance of the network so that the computational efficiency of the DNN scheme significantly exceeds the SPCA scheme. The overall process of the proposed scheme is shown in Fig. 2. we present each step of this process in detail.

A. DNN Structure

The proposed DNN structure is based on multi-layer perceptrons made up of an input layer, multiple hidden layers, and one output layer. The system parameters $\Theta = [\text{Vec}(\mathbf{C}_E), \mathbf{f}_R, \mathbf{g}_R, \mathbf{f}_E, \mathbf{q}_E, N_E, N, \boldsymbol{\kappa}, Q_{tot}, P_T, Q_l]$ with $\boldsymbol{\kappa} = [k_s^t, k_{J_1}^t, k_{J_2}^t, k_D^r, k_R^r, k_R^t]^T$, is fed to the proposed DNN, and $Q = [R_s, P_s, P_{J_1}, \mathbf{w}]$, is obtained at the output. Each neuron receives information from the neurons of the preceding layer according following formula:

$$p_j^{(i+1)} = \xi^{(i)} \left(\sum_{k=1}^{k=N_i} w_{j,k}^{(i)} u_k^{(i)} + b_k^{(i)} \right), \quad (32)$$

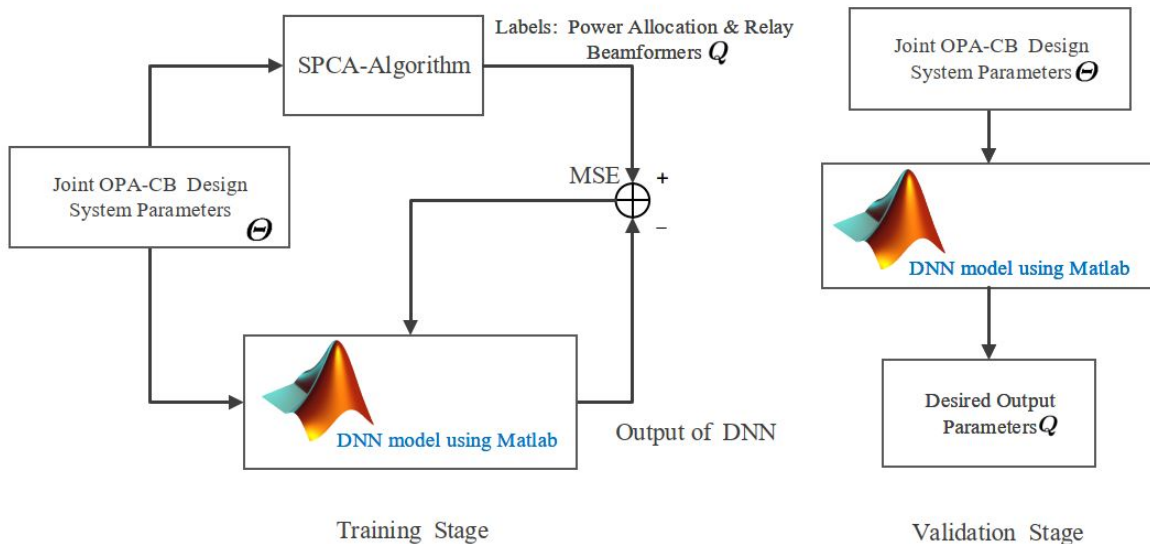


Fig. 4. The training and validation stages of DNN model

where $w_{j,k}^{(i)}$ is a weight that determines relationship between the k -th neuron in i -th layer and j -th neuron in the $(i + 1)$ -th layer. Moreover, $b_k^{(i)}$ is the bias of the neuron associated with the k -th neuron in the $(i + 1)$ -th layer. In the i -th layer, the number of neurons is represented by N_i , and $\xi^{(i)}(\cdot)$ denotes the activation function. Note that the rectified linear unit (ReLU) is a well-suited activation function for such nonlinear regression, and therefore is used in the proposed network. The ReLU function can mitigate the gradient dispersion, which is denoted as $\text{ReLU}(x) = \max(0, x)$.

B. Data Generation Stage

The proposed DNN is trained in an epochal setting, and the input data is generated according to the following procedure. First, the system parameters $\Theta^{(i)}$ are generated, where i represents the i -th training sample. Then, the optimized power allocations and relay beamformer $Q^{(i)}$ are generated using SPCA for each tuple $\Theta^{(i)}$ according to (30) and (31). The i -th training sample is the tuple $\mathcal{H} = \left\{ \left(\Theta^{(i)}, Q^{(i)} \right) \right\}$. We then perform this process K times to generate the validation and training datasets, therefore K is the size of the dataset. Before training the neural network, it is necessary to preprocess the data set with the aim of improving the network generalization ability and reducing the influence of singular values [32]. Accordingly, normalization is carried out prior to training the network [33], and thus the data are

normalized through a standard normal distribution given by:

$$\tilde{\Theta} \triangleq \left\{ \tilde{\Theta}^{(i)} \right\}_{i=1}^K, \quad \tilde{\Theta}^{(i)} = \frac{\Theta^{(i)} - \mu^{(i)}}{\sigma^{(i)}}, \quad (33)$$

where $\tilde{\Theta}^{(i)}$, $\mu^{(i)}$, and $\sigma^{(i)}$ express the normalized value, the mean value and the standard deviation of the i -th training sample, respectively. The proposed DNN framework is shown in Fig. 3.

C. Training Stage

The DNN scheme is shown in Fig. 4, which consists of the training and the validation stages. The training process is responsible for continuously optimizing the weight of the DNN. The adaptive Adam-optimizer is also used aimed at alleviating the burden of debugging parameters such as the learning rate and the batch size. In addition, a dropout method with probability $p = 0.75$ is adopted, which randomly deactivates some neurons with the aim of eliminating the dependency on the output of a specific neuron. The overfitting problem is therefore prevented, resulting in enhancing the model robustness and improving the scalability of the network. Moreover, the decay rate is fixed to 0.9, and the batch size and the learning rate are selected using cross-validation⁵. The goal is to minimize the loss function which reflects the mean square error (MSE) between the label values and the network output values. The training and the validation stages are shown in Fig.4. Moreover, the loss function of the proposed DNN can be rewritten as:

$$\text{MSE} = \min_{\{w_{j,k}^{(i)}\}, \{b_k^{(i)}\}} \sum_j \left(\left\| p_j^{(out)} - Q_j^{(i)} \right\|^2 \right) \quad (34)$$

where $p_j^{(out)}$ and $Q_j^{(i)}$ are the j -th entry of output layer and the label value, respectively. In the training stage of DNN, we update the weight $\left\{ w_{j,k}^{(i)} \right\}_{j,k,i}$ and bias $\left\{ b_k^{(i)} \right\}_{k,i}$ to minimize loss function.

D. Validation Stage

The validation process is necessary to tune the hyperparameters (i.e. the architecture) and provide an unbiased evaluation of the trained DNN fitted on the training dataset. Clearly, the primary goal of the proposed DNN is to achieve the best performance on a new dataset. As a result, the simplest approach to evaluate the performance of the proposed DNN is to assess the MSE using the data independent of those

⁵A dataset can be repeatedly split into a training dataset and a validation dataset, known as cross-validation. These repeated partitions can be done in various ways such as dividing into 2 equal datasets, and using them as training/validation, and then validation/training, or repeatedly selecting a random subset as a validation dataset [30]. To validate the model performance, sometimes an additional test dataset that was held out from cross-validation is used.

used in the training stage. we pass the validation set to the network and then we get the output of the DNN model. Then, the MSE of the system is calculated using the label values and the output values.

VI. COMPLEXITY ANALYSIS

In this subsection, we aim to compare the complexity order of SPCA-based and the DNN-based schemes, respectively. The overall proposed SPCA-based scheme involves the Algorithm 1 and the FIPSA Algorithm 2. As both Algorithm 1 and Algorithm 2 (Eq. (30) and (31)) have analogous structures, calculating the complexity order of only Algorithm 1 is sufficient. The optimization problem (30), used in Algorithm 1, is a semidefinite programming (SDP), whose all the constraints were transformed into LMIs by using Schur complements. Even though it is not a standard SDP problem [21], using the interior-point method, the worst-case complexity can be calculated by $\mathcal{O}(m^2(\sum_i m_i^2)\sqrt{\sum_i m_i})$, where m is the number of optimization variables and m_i is the dimension of the i -th semidefinite cone [34]. Therefore, when the interior-point method is employed to solve the problem (30), the worst-case computational complexity at each iteration can be calculated by:

$$\zeta_{\text{SPCA}} \triangleq \mathcal{O}\left((N-N_E)^2(2(N-N_E+1)^2+(N_E+1)^2)\sqrt{2(N-N_E+1)+(N_E+1)}\right), \quad (35)$$

If we let T_1 and T_2 respectively denote the required numbers of iterations for SPCA and FIPSA algorithms, the overall complexity order is calculated by (T_1+T_2) times of ζ_{SPCA} . On the other hand, The proposed DNN-based scheme relies on supervised learning regression algorithm, comprised of different number of hidden layers and nodes per layer. The time complexity of DNN can be represented by floating-point operations (FLOPs) [26]. For each layer of the neural network, the number of FLOPs can be expressed as:

$$\text{FLOPs}_i \triangleq 2I_iO_i \quad (36)$$

where I_i is the input dimension of the i -th layer and O_i is the output dimension of the i -th layer. Therefore, for our supervised learning scheme, the number of FLOPs is:

$$\zeta_{\text{DNN}} = \sum_{i=1}^{i=3} \text{FLOPs}_i = 2((2 \times (N+N_E) + N_E \times N + 5)N_1 + N_1N_2 + (3 + N_2 + N)N_3), \quad (37)$$

where N_i , $i = 1, 2, 3$ is the neurons number of i -th hidden layer. Comparing ζ_{SPCA} and ζ_{DNN} , it can be explicitly seen that: $\zeta_{\text{DNN}} \ll \zeta_{\text{SPCA}}$, as we expected.

TABLE I
SUMMARY OF THE PROPOSED DNN STRUCTURE AND NOTATIONS

Symbols	Values
Training epoch	400
Batch size	32
Learning rate	10^{-3}
Decay rate	0.9
The size of training dataset	9×10^3
The size of validation dataset	10^3
The input dimension	$2 \times (N + N_E) + N_E \times N + 5$
The output dimension	$N + 3$
The number of neurons in the 1 th layer: N_1	256
The number of neurons in the 2 th layer: N_2	256
The number of neurons in the 3 th layer: N_3	128
Dataset size: K	10^4
Dropout: p	0.75

VII. SIMULATION RESULTS

In this section, we assess the proposed schemes using simulations. Our simulation setting is based on the following adjustment, unless otherwise stated. The threshold values for the stopping criteria of Algorithm 1 and of FIPSA are respectively $\delta_I = \delta_\epsilon = 10^{-3}$, the impairments at each node are $k_i^t = k_i^r = 0.08$, the number of antennas at Eve is $N_E = 2$, the Gaussian noise power $\sigma^2 = 10^{-3}$, $Q_{tot} = 30$ dB, $P_T = 1.5 Q_{tot}$, $N = 12$ and $Q_l = \frac{2Q_{tot}}{N}$. All simulations were averaged over 1000 independent channel realizations. The parameters of DNN are set as shown in Table I. The proposed DNN framework is shown in Fig. 3. This network contains one input layer, three hidden layers and one output layer, where the three hidden layers have 256, 256 and 128 neurons. The validation set is utilized to measure the computing performance and ASR of DNN and the training set is used for model training. The proposed scheme is performed in MATLAB 2019b, with Intel(R) Core(TM) i7-7700@3.6GHz, NVIDIA GeForce GTX 1080.

Fig. 5 depicts the average convergence of the proposed FIPSA algorithm. As it can be clearly seen, the average convergence of FIPSA is fast, such that regardless to the number of relays, it rapidly converges at the second iteration. The average convergence speed of the proposed SPCA-based solution for the problem in (25) is shown in Fig. 6. The results show. the convergence of (31) at almost 10 iterations for any feasible points. Similar to the convergence behavior of FIPSA, there is no relationship between the convergence behavior and the number of relay nodes, which confirms the practicality of our proposed

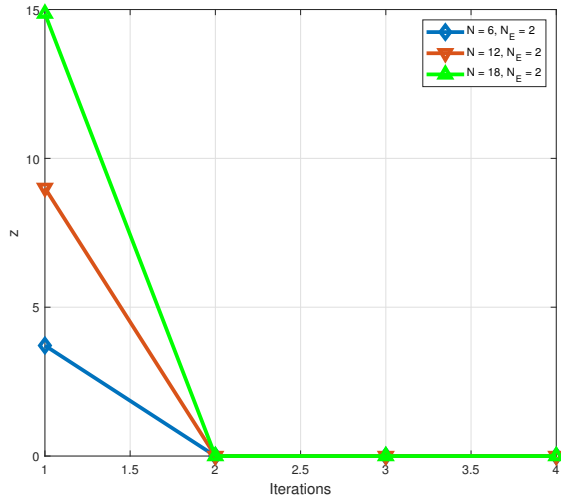


Fig. 5. Evaluating of convergence behavior of the FIPSA through depicting the OF value in (31) versus the number of iterations for $N = 6, 12, 18$ and $N_E = 2$

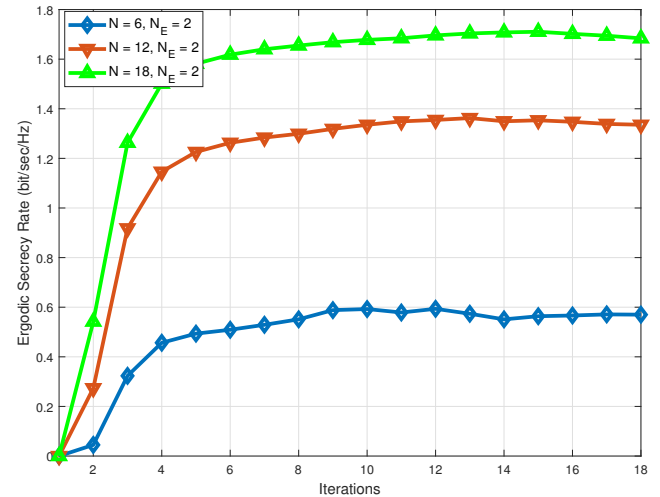


Fig. 6. Average Ergodic secrecy rate R_s achieved by the proposed algorithm versus the number of iterations for $N = 6, 12, 18$ and $N_E = 2$

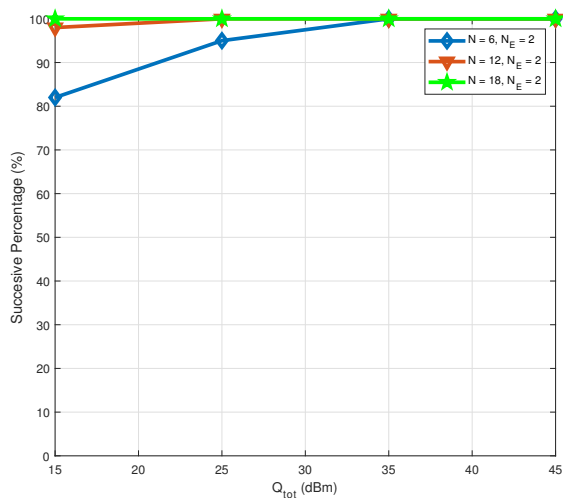


Fig. 7. Percentage of successful cases versus total power budget Q_{tot} for $N = 6, 12, 18$ and $N_E = 2$

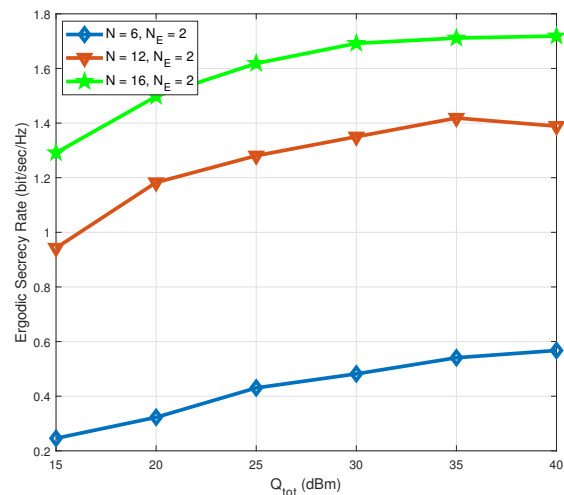


Fig. 8. Average Ergodic secrecy rate R_s achieved versus the total power budget Q_{tot} for $N = 6, 12, 18$ and $N_E = 2$

algorithm.

In Fig. 7, we depict the percentage of successful cases achieved by FIPSA versus Q_{tot} for different N . Simulation results show that with increasing N and Q_{tot} , the percentage of successful cases increases. Actually, it can be interpreted that, by increasing available resources, i.e., transmit power and spatial degree of freedom (DOF), the feasibility of the non-convex problem (25) would be improved. Fig. 8 shows the average secrecy rate achieved by SPCA versus the total power budget for different number of relays. This figure states that as the total power becomes high, the average secrecy rate is confined to a

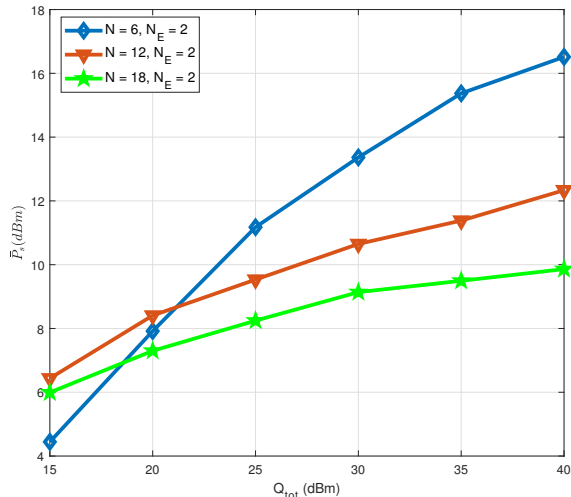


Fig. 9. Average source power consumption P_s versus the total power budget Q_{tot} for $N = 6, 12, 18$ and $N_E = 2$

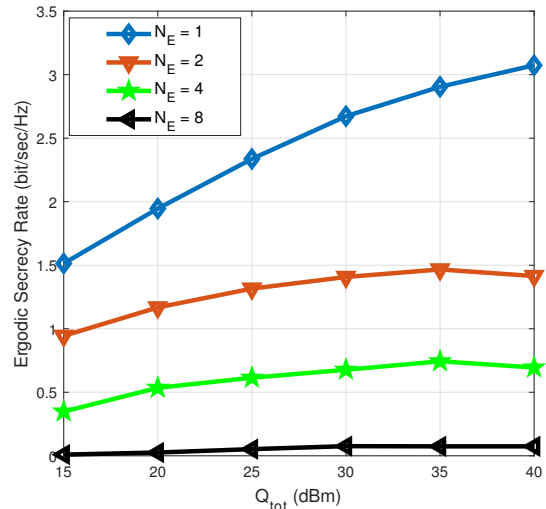


Fig. 10. Ergodic secrecy rate R_s versus the total power budget Q_{tot} for $N = 12$ and $N_E = 1, 2, 4, 8$

ceiling due to presence of impairments. We can also observe that given a specific total power budget, the secrecy rate increases as the number of relays grows. This is because by increasing the number of relays, the network's degree of freedom is increased, hence enhancing the ASR.

Observe in Fig. 9, the power consumed by the source for information transmission is reduced upon increasing the number of untrusted relays. This observation is originated from two different reasons. On one hand, by increasing the number of untrusted relays, the information leakage at phase I is increased. Consequently, to safeguard the information, most of the total power must be assigned for jamming, and thus the remaining power for transmitting the information is decreased. On the other hand, upon increasing N , more degrees of freedom is provided for the relay nodes which improves their capability to do beamforming. Hence, there is no need for increasing P_s . However at low power budget regimes most of the power is allocated to relay nodes to perform beamforming. This will lead to more tangible impacts of HIs at relay nodes. As a consequence of this intrinsically AN emitted by imperfect relay nodes, less power is allocated to jamming signal and most of the total power budget is preferred to be assigned for information transmission.

The impact of number of the antennas deployed at Eve is shown in Fig. 10. As it would be expected, given a fixed number of relays and a specific total power budget, the average secrecy rate is decreased upon increasing N_E . This is because, deploying more antennas at the eavesdropper makes it stronger to decipher the information and hence degrade the secrecy.

Fig. 11 depicts the power consumed at source and jammer nodes versus the number of relay nodes.

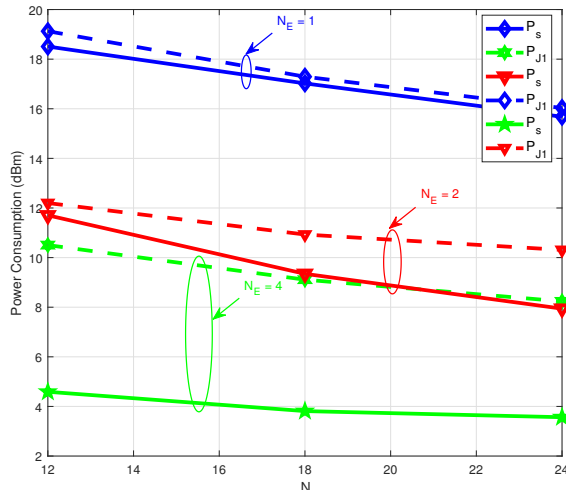


Fig. 11. Average source and friendly jammer power consumption P_s, P_{J1} versus the total number of relay nodes N for $N_E = 1, 2, 4$

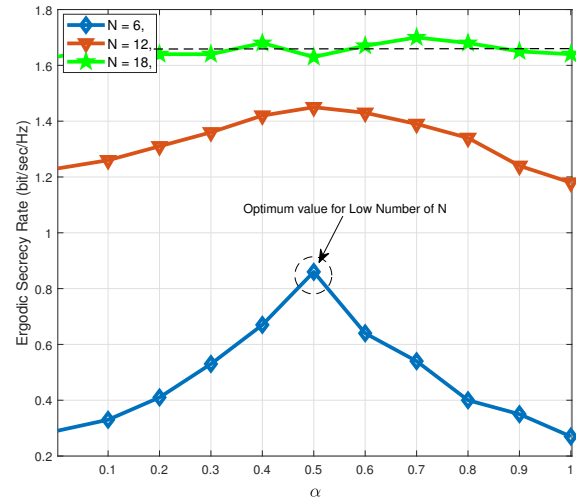


Fig. 12. Average Ergodic secrecy rate R_s versus different values of impairments at relay nodes for $k_R^t = \alpha, k_R^r = 0.2(1 - \alpha), k_S^t = k_D^r = 0.1, N = 6, 12, 18$ and $N_E = 2$

The results were displayed for various numbers of antennas deployed at Eve. Observe in Fig. 11, the difference between P_s and P_{J1} is increased upon increasing the number of antennas deployed at Eve. This is because, by increasing N_E the secrecy is more degraded, and hence more jamming power is required to confront eavesdropping attacks accomplished via external Eve. Another interesting observation from Fig. 11 is that the impact of N_E on power consumption at source and jammer is much more considerable than that of the number of cooperative relays. In other words, the impact of N_E is dominant as compared with the number of untrusted relay nodes. The reason for this is that increasing N_E results in purely degrading the security. However, increasing the number of untrusted relays, although the security may be jeopardized, the provided DoF together with emitted artificial noise due to inherent impairment of relay nodes can boost the secrecy rate, on the other hand. In order to design a practical secure network we need the engineering perspective of how the total tolerable hardware impairment at each relay node should be distributed between the RF reception and RF transmission segments to maximize the secrecy rate. Actually, depending on the specified expense we aim to spend, it is needed to know how the RF chain at the transmission and reception front ends of each relay node should be designed to reach the abovementioned goal. In this respect, the distribution parameter $0 < \alpha < 1$ is defined such that we have $\alpha k_R^r + (1 - \alpha) k_R^t = 0.2$. Through this definition, depending the value of α , the total impairment level of 0.2, considered at each relay node, is divided between the transmission and reception sections of the same node. Observing Fig. 12, it can be explicitly seen that in the case of using low number of relays,

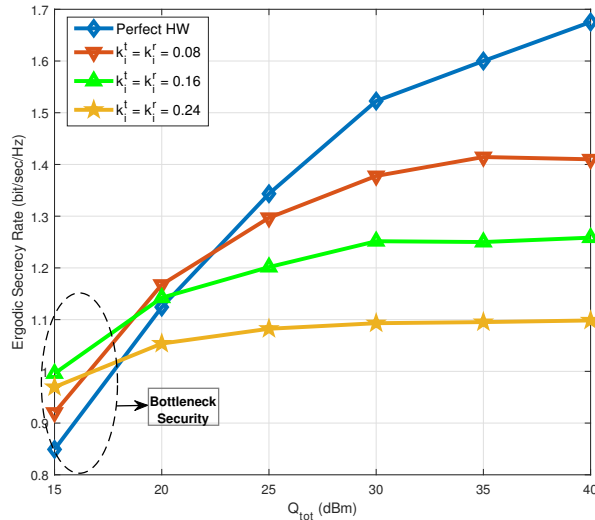


Fig. 13. Average Ergodic secrecy rate R_s versus the total power budget Q_{tot} for different values of hardware impairments, $N = 12$ and $N_E = 2$

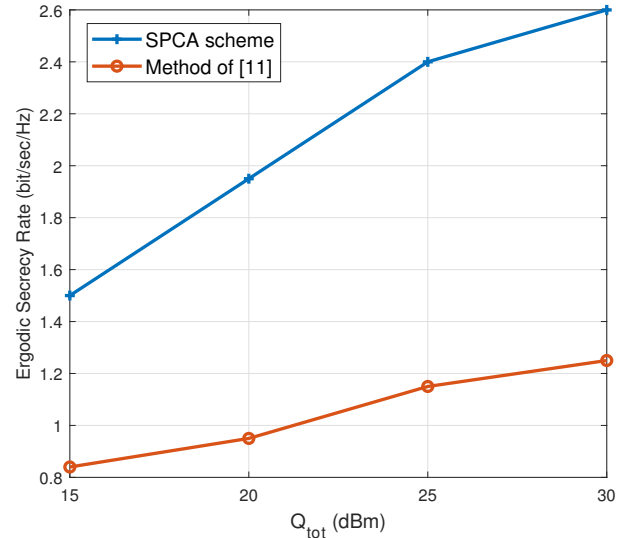


Fig. 14. Average Ergodic secrecy rate R_s versus the total power budget Q_{tot} for minimum quality of service of $\gamma_{min} = 12$ dB

it is favored to expend our budget at the reception and transmission front ends equally. This intuitive result has been mathematically analyzed in [14], as well. By doing so, both the RF reception and RF transmission experiences equal levels of impairment. However, upon increasing the number of relays, the network secrecy performance will be independent of the network HIs. This is due to the fact that the network's DoF is enhanced upon increasing the number of relays.

The impact of impairment levels on the ASR is demonstrated in Fig. 13. As it can be observed, at high power budgets, the more the hardware are impaired, the less secrecy rate is acquired. In contrast, at low power budgets, which there exists a low power to be allocated for jamming signals, the artificial noise due to impairment plays the role of jamming. As a consequence, upon increasing the impairment level, it is preferred to allocate the major part of the power to the source and let the inherent artificial noise due to impairment assist in safeguarding the communication. Hence it is no longer expected to have lower secrecy rate upon increasing the impairment levels at low power budgets.

As mentioned before, the method presented in this paper was designed for the case where we have perfect knowledge about external Eve. The resultant maximization problem on secrecy rate, led to SPCA solution, can be regarded as the upper bound. In contrast, if we assume no knowledge about the external Eve (as already considered in [11], another secrecy scheme should be adopted, leading to a sub-optimal solution which has considerably inferior performance than ours (as it can be clearly seen in Fig.14). For a fair comparison, the minimum QoS, $\gamma_{min} = 12$ dB, has been considered.

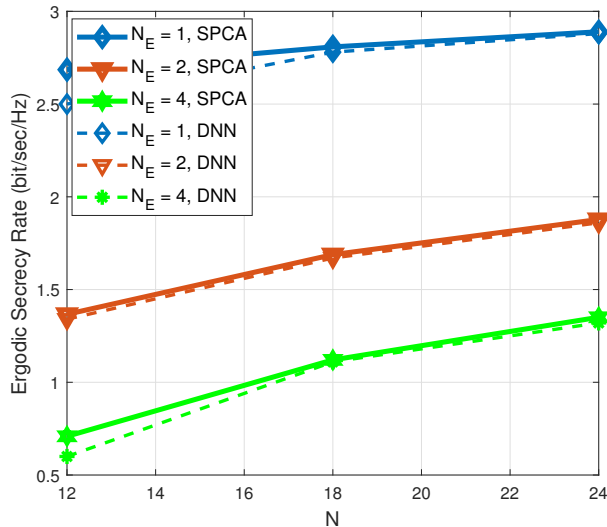


Fig. 15. Ergodic secrecy rate of the proposed DNN scheme and the SPCA-based scheme versus the total number of relay nodes N

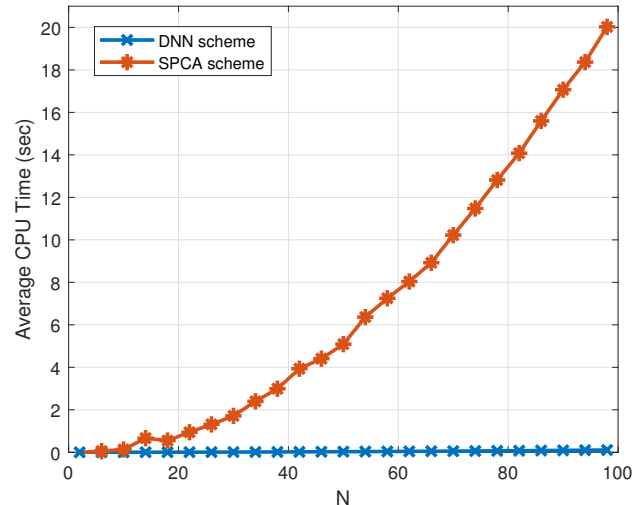


Fig. 16. Average CPU time of the proposed DNN scheme and the sub-optimal scheme (SPCA) versus the total number of relay nodes N

Fig. 15 reveals the comparison result of our proposed DNN-based scheme with SPCA-based scheme. We evaluate the ergodic secrecy rate versus total number of untrusted relay nodes N . Observing Fig. 15, we can find that our DNN model provides a very accurate prediction of the ASR, such that for $N = 24$ the DNN-based scheme can achieve 99.61% ASR performance of SPCA-based scheme.

As discussed before, DL can deal with the imposed computational load upon increasing the network's dimensions, making it an appropriate choice to satisfy the low-latency requirement of B5G. In this respect, Fig. 16 shows the average CPU time versus the number of relay nodes for the proposed DNN-based and SPCA-based schemes. It can be clearly seen that, the DNN-based scheme requires the average CPU time much less than SPCA-based scheme. For instance, when total number of relay nodes power is 100, the average CPU time of the proposed DNN-based scheme is 0.0031 sec but that of SPCA-based is 20.934 sec, which is approximately 6,752.9 times. Specifically, as number of relay nodes N increases, the average CPU time of the DNN-based scheme remains nearly constant but that of SPCA-based grows exponentially due to an increasing number of iterations.

Fig. 17 shows that unlike the assumption of unknown Eve's CSI in [11], which a relay selection algorithm, known as hybrid assisted cooperative jamming (HACJ), was required to improve the secrecy, we can get rid of the computational load imposed by relay selection using simple DACJ, achieving the performance even better than HACJ. This is because, assuming perfect CSIT and CSIR, instead of choosing a relay node as a jammer the entire potential of relay nodes are preferred to forming a centralized beam

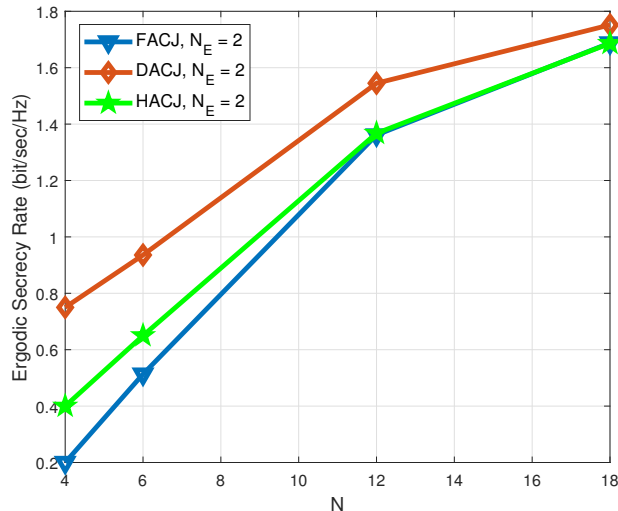


Fig. 17. Ergodic secrecy rate of the proposed SPCA scheme versus the total number of relay nodes N and different jammer selection scheme

towards the legitimate destination whilst completely nulling out the leakage at Eve.

VIII. CONCLUSIONS

This paper has investigated PLS of an untrusted relaying network in the face of realistic hardware impairment, where the source node communicates in the presence of a multi-antenna Eve. The network relies on untrusted relay nodes for increasing its communications quality, while aiming for preserving the confidentiality of the information against the combined eavesdropping attacks performed by both the untrusted relays and a single Eves. We have assumed perfect CSIT and CSIR. This assumption was indeed a strong one, hence the results represent the best-case performance limit of practical relaying in the presence of HIs. In this regard, the relay beamformer and the transmit powers were jointly optimized to maximize the ASR under both the total and individual power budget constraints of the entire network and each nodes, respectively. Moreover, DACJ was employed to safeguard the first cooperative phase. On the other hand, for the second phase, the relay beamformer was adjusted for ensuring that the information leakage at Eve is entirely removed. The resultant optimization problem was non-convex and solved efficiently using the SPCA method. In order to prevent any failure due to the solution's infeasibility, we have also proposed an iterative initialization algorithm to find an initial point of the original problem, leading to a feasible solution instead of relying on an arbitrary point. Furthermore, to facilitate the implementation of proposed algorithm in large-scale scenarios relying on numerous relays, a computationally efficient data-driven approach was developed. A DL model was developed to maximize the ASR performance,

while the computational burden is significantly reduced. Through extensive simulation results, we have examined the effect of different system parameters on the ASR performance as well as the efficiency of the proposed DL solution in large-scale scenarios.

REFERENCES

- [1] Mukherjee, Amitav and Fakoorian, S Ali A and Huang, Jing and Swindlehurst, A Lee, "Principles of physical layer security in multiuser wireless networks: A survey." *IEEE Communications Surveys & Tutorials*, 16(3), pp. 1550–1573, 2014. IEEE.
- [2] Wyner, Aaron D, "The wire-tap channel" *Bell system technical journal*, 54(8), pp. 1355–1387, 1975. Wiley Online Library.
- [3] Wang, Chao and Wang, Hui-Ming and Xia, Xiang-Gen, "Hybrid opportunistic relaying and jamming with power allocation for secure cooperative networks". *IEEE Transactions on Wireless Communications*, 14(2), pp. 589–605, 2014. IEEE.
- [4] Wang, Chao and Wang, Hui-Ming and Xia, Xiang-Gen, "Hybrid opportunistic relaying and jamming with power allocation for secure cooperative networks". *IEEE Transactions on Wireless Communications*, 14(2), pp. 589–605, 2014. IEEE.
- [5] Wang, Hui-Ming and Luo, Miao and Yin, Qinye and Xia, Xiang-Gen, "Hybrid cooperative beamforming and jamming for physical-layer security of two-way relay networks". *IEEE Transactions on Information Forensics and Security*, 8(12), pp. 2007–2020, 2013, IEEE.
- [6] Wang, Hui-Ming and Liu, Feng and Yang, Mengchen, "Joint cooperative beamforming, jamming, and power allocation to secure AF relay systems". *IEEE Transactions on Vehicular Technology*, 64(10), pp. 4893–4898, 2015. IEEE.
- [7] Yang, Ye and Li, Qiang and Ma, Wing-Kin and Ge, Jianhua and Ching, PC, "Cooperative secure beamforming for AF relay networks with multiple eavesdroppers". *IEEE Signal Processing Letters*, 20(1), pp. 35–38, 2013. IEEE.
- [8] Moradikia, Majid and Mashdour, Saeed and Jamshidi, Ali, "Joint optimal power allocation, cooperative beamforming, and jammer selection design to secure untrusted relaying network". *Transactions on Emerging Telecommunications Technologies*, 29(3), pp. e3276, 2018. Wiley Online Library.
- [9] Y. Wang. and Z. Shi, "Channel reciprocity and capacity analysis with outdoor MIMO measurements". *IEEE 18th International Workshop on Signal Processing Advances in Wireless Communications (SPAWC)*, 2017.

- [10] E. Bjornson and M. Matthaiou and M. Debbah, "A New Look at Dual-Hop Relaying: Performance Limits with Hardware Impairments". *IEEE Transactions on Communications*, pp. 4512-4525, 2013.
- [11] M. Moradikia and H. Bastami and A. Kuhestani and H. Behroozi and L. Hanzo, "Cooperative Secure Transmission Relying on Optimal Power Allocation in the Presence of Untrusted Relays, A Passive Eavesdropper and Hardware Impairments". *IEEE Access*, pp.116942-116964, 2019.
- [12] Ouyang, Nian and Jiang, Xue-Qin and Bai, Enjian and Wang, Hui-Ming, "Destination assisted jamming and beamforming for improving the security of AF relay systems". *IEEE Access*, pp. 4125–4131, 2017. IEEE.
- [13] Zarrabi, Houman and Kuhestani, Ali and Moradikia, Majid, "EE-RS and PA for untrusted relay network at high signal-to-noise ratio regime". *IET Communications*, 10(16), pp. 2143–2148, 2016, IET.
- [14] A. Kuhestani and A. Mohammadi, K. Wong, P. L. Yeoh, M. Moradikia, and M. R. A. Khandaker, "Optimal Power Allocation by Imperfect Hardware Analysis in Untrusted Relaying Networks". *IEEE Transactions on Wireless Communications*, pp. 4302-4314, 2018.
- [15] S. Mashdour, M. Moradikia, and P. L. Yeoh, "Secure mm-wave communications with imperfect hardware and uncertain eavesdropper location", arXiv:2005.05439, 2020.
- [16] H. Ruan and R. C. de Lamare, "Distributed robust beamforming based on low-rank and cross-correlation techniques: Design and analysis," *IEEE Transactions on Signal Processing*, vol. 67, no. 24, pp. 6411-6423, 2019.
- [17] M. Atallah and G. Kaddoum, "Secrecy capacity scaling with untrustworthy aggressive relays cooperating with a wire-tapper," *IEEE Wireless Communications Letters*, vol. 5, no. 4, pp. 376-379, 2016.
- [18] Mukherjee and A. L. Swindlehurst, "Detecting passive eavesdroppers in the MIMO wiretap channel," in *2012 IEEE International Conference on Acoustics, Speech and Signal Processing (ICASSP)*, 2012, pp. 2809-2812.
- [19] B. R. Marks and G. P. Wright, "A general inner approximation algorithm for nonconvex mathematical programs," *Operations Research*, vol. 26, no. 4, pp. 681-683, 1978. [Online]. Available: <http://www.jstor.org/stable/169728>
- [20] A. Beck, A. BenTal, and L. Tetrushvili, "A sequential parametric convex approximation method with applications to nonconvex truss topology design problems," *Journal of Global Optimization*, vol.

- 47, no. 1, pp. 29-51, May 2010. [Online]. Available: <https://doi.org/10.1007/s10898-009-9456-5>
- [21] S. Boyd and L. Vandenberghe, *Convex Optimization*. USA: Cambridge University Press, 2004.
- [22] D. Bertsekas, *Nonlinear Programming*. Athena Scientific, 1999.
- [23] O. Dizdar, Y. Mao, W. Han, and B. Clerckx, "Rate-splitting multiple access: A new frontier for the Phy layer of 6G," 2020.
- [24] T. Schenk, *RF imperfections in high-rate wireless systems: Impact and digital compensation*, 01 2008.
- [25] C. Wang, H. Wang, D. W. K. Ng, X. Xia, and C. Liu, "Joint beamforming and power allocation for secrecy in peer-to-peer relay networks," *IEEE Transactions on Wireless Communications*, vol. 14, no. 6, pp. 3280-3293, 2015.
- [26] N. Yang, H. Zhang, K. Long, H. Hsieh, and J. Liu, "Deep neural network for resource management in NOMA networks," *IEEE Transactions on Vehicular Technology*, vol. 69, no. 1, pp. 876-886, 2020.
- [27] H. Sun, X. Chen, Q. Shi, M. Hong, X. Fu, and N. D. Sidiropoulos, "Learning to optimize: Training deep neural networks for interference management" *IEEE Transactions on Signal Processing*, vol. 66, no. 20, pp. 5438-5453, 2018.
- [28] H. He, C. Wen, S. Jin, and G. Y. Li, "Deep learning-based channel estimation for beamspace mmwave massive MIMO systems," *IEEE Wireless Communications Letters*, vol. 7, no. 5, pp. 852-855, 2018.
- [29] P. de Kerret, D. Gesbert, and M. Filippone, "Team deep neural networks for interference channels," *in 2018 IEEE International Conference on Communications Workshops (ICC Workshops)*, 2018, pp. 1-6.
- [30] R. Kohavi, "A study of cross-validation and bootstrap for accuracy estimation and model selection," vol. 14, 03 2001.
- [31] W. Lee, M. Kim, and D. Cho, "Deep power control: Transmit power control scheme based on convolutional neural network," *IEEE Communications Letters*, vol. 22, no. 6, pp. 1276-1279, 2018.
- [32] C. V. Gonzalez Zelaya, "Towards explaining the effects of data preprocessing on machine learning," *in 2019 IEEE 35th International Conference on Data Engineering (ICDE)*, 2019, pp. 2086-2090.
- [33] P. Ferreira, D. C. Le, and N. Zincir-Heywood, "Exploring feature normalization and temporal information for machine learning based insider threat detection," *in 2019 15th International Conference on Network and Service Management (CNSM)*, 2019, pp. 1-7.
- [34] J. F. Sturm, "Implementation of interior point methods for mixed semidefinite and second order cone

- optimization problems," *Optimization Methods and Software*, vol. 17, no. 6, pp. 1105-1154, 2002. [Online]. Available: <https://doi.org/10.1080/1055678021000045123>
- [35] H. Zhang, H. Zhang, K. Long, and G. K. Karagiannidis, "Deep learning based radio resource management in noma networks: User association, subchannel and power allocation," 2020.
- [36] H. Guo, Z. Yang, Y. Zou, T. Tsiftsis, M. R. Bhatnagar, and R. C. D. Lamare, "Secure beamforming for cooperative wireless-powered networks with partial CSI," *IEEE Internet of Things Journal*, vol. 6, no. 4, pp. 6760-6773, 2019.
- [37] H. Wu, Y. Zou, W. Cao, Z. Chen, T. A. Tsiftsis, M. R. Bhatnagar, and R. C. De Lamare, "Impact of hardware impairments on outage performance of hybrid satellite-terrestrial relay systems," *IEEE Access*, vol. 7, pp. 35 103-35 112, 2019.
- [38] X. Chen, D. Li, Z. Yang, Y. Chen, N. Zhao, Z. Ding, and F. R. Yu, "Securing aerial-ground transmission for NOMA-UAV networks," *IEEE Network*, pp. 1-7, 2020.
- [39] L. Lv, H. Jiang, Z. Ding, L. Yang, and J. Chen, "Secrecy-enhancing design for cooperative downlink and uplink NOMA with an untrusted relay," *IEEE Transactions on Communications*, vol. 68, no. 3, pp. 1698-1715, 2020.
- [40] C. Wang, Z. Li, J. Shi, J. Si, and D. W. K. Ng, "Physical layer security of vehicular networks: A stochastic geometry approach," in *2020 IEEE International Conference on Communications Workshops (ICC Workshops)*, 2020, pp. 1-7.
- [41] J. Liu, K. Xiong, Y. Lu, D. W. K. Ng, Z. Zhong, and Z. Han, "Energy efficiency in secure IRS-aided SWIPT," *IEEE Wireless Communications Letters*, pp. 1-1, 2020.